Available online at www.sciencedirect.com
ScienceDirect
Prog. Polym. Sci. 32 (2007) 1462–1498
PROGRESS IN POLYMER SCIENCE
www.elsevier.com/locate/ppolysci

New phosphate glass/polymer hybrids—Current status and future prospects

Kevin Urman, Joshua U. Otaigbe*

School of Polymers and High Performance Materials, The University of Southern Mississippi, 118 College Drive #10076, Hattiesburg, MS 39406, USA

Received 9 May 2007; received in revised form 26 July 2007; accepted 26 July 2007
Available online 21 August 2007

Abstract

The physical modification of polymer structure and properties via polymer blending and reinforcement is a common practice in the plastics industry and has a large economic advantage over synthesizing new polymeric materials to fulfill new material needs. In this context, a new class of inorganic glass/organic polymer hybrids with enhanced benefits has been recently developed by blending low-Tg phosphate glasses with polymeric materials in the liquid state, to afford new hybrid materials with significant improvements in properties that are impossible to achieve from classical polymer blends and composites. Because of their facile synthesis and desirable characteristics, these phosphate glass/polymer hybrid materials may be model systems for exploring feasibility of new routes for driving inorganic glasses and organic polymers to self-assemble into useful materials. Conceptually, it may even be possible to use block copolymers, with one block being miscible with Pglass, to perform self-directed assembly of nanostructured hybrids, where the Pglass is confined solely to one phase. This article reviews some new insights into the structural dynamics, melt rheology, molecular relaxation processes, and phase behavior of a few representative examples of these unique hybrid materials with prescribed rheological properties, macromolecular structure and function. The unanswered questions are discussed to guide future research directions, and facilitate progress in this emerging area.

Keywords: Hybrid organic/inorganic polymers; Polyphosphate glass; Structure and properties; Rheology

Contents

*Corresponding author. Tel.: +1 601 266 5596; fax: +1 601 266 5504.
E-mail address: Joshua.Otaigbe@usm.edu (J.U. Otaigbe).

0079-6700/$ - see front matter © 2007 Elsevier Ltd. All rights reserved.
doi:10.1016/j.progpolymsci.2007.07.006

1. Introduction

Conventional multiphase polymeric materials such as polymer blends and composites play a vital role in fulfilling the world's material needs. The importance of these materials has spawned significant industrial and academic interest. The ability to predict and tailor the properties of polymer blends gives them a significant economic advantage over synthesizing a new material to meet the specific requirements of a desired application, leading to the large growth of the polymer blend industry over the past 20 years [1,2]. As an additional benefit, blending two or more polymers can have synergistic effects that create a substantially better material than the pure polymer components. These improved properties can include reduced viscosities and enhanced mechanical properties [3–7].

However, classical polymer blends and composites cannot meet all of the material needs for new technological advances despite their wide range of properties. Inorganic/organic hybrid materials are helping to bridge this gap. Hybrid inorganic/organic materials are broadly defined as synthetic materials with organic and inorganic components. Strictly speaking, an inorganic/organic hybrid is a material that consists of separate regions dominated by either the inorganic or organic component and the resultant hybrid material displays properties that are not a linear average of these regions [8]. The high degree of control over the composition and structure in hybrid materials results in vastly improved, tunable properties relative to that of the pure inorganic or organic components [9]. Hybrids can be further classified into two types: i.e., homogeneous and heterogeneous. Homogeneous hybrid systems are derived from monomers or miscible inorganic/organic components, while the heterogeneous systems are phase-separated and display domains with sizes ranging from angstroms to micrometers [9].

Traditionally, homogeneous hybrid systems are prepared through the sol–gel process [10]. The sol–gel process is basically a series of hydrolysis and condensation reactions of a metal alkoxide species in which a network is eventually formed [11]. The general reaction scheme for the sol–gel process is shown in Fig. 1 [11]. Hybrid inorganic/organic materials are prepared from the sol–gel reaction by incorporating functionalized monomers or oligomers that can react with the hydrolysis products of the metal alkoxide. This process results in a hybrid with the organic polymer dispersed without aggregation in the hybrid matrix [12]. Additionally, the inorganic component is often dispersed on the nanometer length scale due to the covalent bonds or physical interactions between the polymer and inorganic phase, which leads to a range of unique properties [13]. Often, these hybrids display high flexibility, transparency, versatility in the design of functional groups, high tensile strength, good gas barrier, and improved thermal and mechanical stability [8,10,13,14]. Unfortunately, commercial applications of sol–gel hybrids are presently limited because they are difficult to fabricate and have expensive, toxic precursor chemicals with high volatile organic compound content. In addition, hybrid materials from sol–gels are often porous and crack or severely contract to squeeze out the incorporated organics when solvents in the gels are evaporated as reported by Niida et al. [15].

Heterogeneous hybrid systems include polymer/clay nanocomposites (PNC) and conventional glass/ceramic polymer composites. Conventional composites are typically prepared by melt mixing a rigid, solid inorganic glass with an organic polymer. These composites offer some improvement in properties at low cost. However, they are often heavy and brittle, and at high glass loadings ($\geqslant 30$ wt%) their melt viscosity becomes intractable, making their

$$\mathrm{Si(OR)_4 + H_2O \rightleftharpoons (HO)Si(OR)_3 + ROH}$$

$$\mathrm{(HO)Si(OR)_3 + H_2O \rightleftharpoons (HO)_2Si(OR)_2 + ROH}$$

$$\mathrm{(HO)_2Si(OR)_2 + H_2O \rightleftharpoons (HO)_3Si(OR) + ROH}$$

$$\mathrm{(HO)_3Si(OR) + H_2O \rightleftharpoons Si(OH)_4 + ROH}$$

$$\mathrm{\equiv Si-OR + HO-Si\equiv \rightleftharpoons \equiv Si-O-Si\equiv + ROH}$$

$$\mathrm{\equiv Si-OH + HO-Si\equiv \rightleftharpoons \equiv Si-O-Si\equiv + HOH}$$

Fig. 1. Reaction scheme for the sol–gel reaction.

processing difficult. PNCs are typically composed of layered silicate clay dispersed inside a polymer matrix. The clay is composed of platelets that are about 1 nm thick and 100–150 nm in length [16,17]. Each of these layers is separated by an intergallery distance which is typically less than 10 nm [16]. This gallery is filled by cations which can be exchanged to facilitate the separation of the stacks and adhesion to the polymer matrix as shown in Fig. 2 [18]. Conceptually, these layered silicates are analogous to a stack of cards. By getting the cards to separate, i.e. exfoliate, completely, optimal property improvements are achieved. However, this is not always possible and an intercalated PNC is achieved [18]. Intercalated PNCs are obtained when the polymer chain inserts itself between the clay platelets, but does not disrupt the overall stack morphology. The properties of intercalated PNCs usually are similar to those of ceramic materials.

PNCs offer extraordinary mechanical property improvements such as strength and tensile modulus without sacrificing impact strength [16]. They also display increased thermal stability, improved flame resistance, and increased barrier properties. All of these property improvements are realized at low clay loadings of $\leqslant 5$ wt%. Due to their properties, PNCs have found widespread uses as advanced structural materials. PNCs do have a disadvantage in that the inorganic phase has a fixed morphology. Because the morphology of a material has a huge impact on the material's properties, it would be desirable to have a material with the ability to tailor the morphology during fabrication. By doing this, the properties of the material could easily be tuned to meet any targeted specifications.

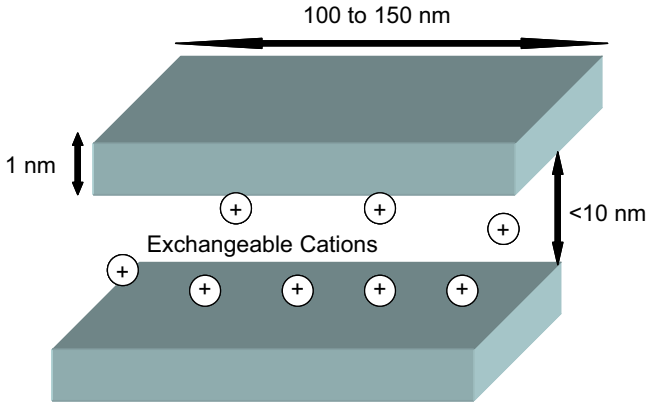

Fig. 2. Schematic of the size scales and exchangeable cations in layered silicate clay.

An example of a relatively new class of inorganic/organic hybrid material that is intermediate between heterogeneous and homogeneous hybrids are phosphate glass (Pglass)/polymer hybrids. These unique hybrid materials are prepared by melt blending a low-T_g inorganic phosphate glass with an organic polymer. Unlike the sol–gel hybrids, these materials do not require expensive, toxic chemical precursors, and the morphology of the inorganic phase is not fixed, like PNCs. It is also possible to incorporate up to 60 vol% (i.e., 90 wt%) of the Pglass component in the hybrid using conventional polymer processing methodologies without the intractable viscosity problem inherent to classical polymer composites at significantly lower inorganic filler concentration. Further, the Pglass/polymer hybrids exhibit all the benefits of traditional filled plastics but without their disadvantages already discussed.

Phosphate glass plays an important role in these novel hybrid systems. A brief overview of phosphate glasses is given here in order to facilitate the understanding of their importance in Pglass/polymer hybrids. Inorganic phosphate glasses are generally considered to be polymeric in nature [19–22]. This is due to the fact that they are composed of chain-like or crosslinked structures that are very similar to polymer chain networks [20]. However, these chains are much shorter than organic polymer chains and often an alkali metal cation aids in the network formation. The building blocks of the phosphate glass networks are the phosphate anion tetrahedra that result from the formation of sp^3 hybrid orbital by the phosphorous outer electrons [19]. These tetrahedra are named according to a Q^i scheme as shown in Fig. 3, where i

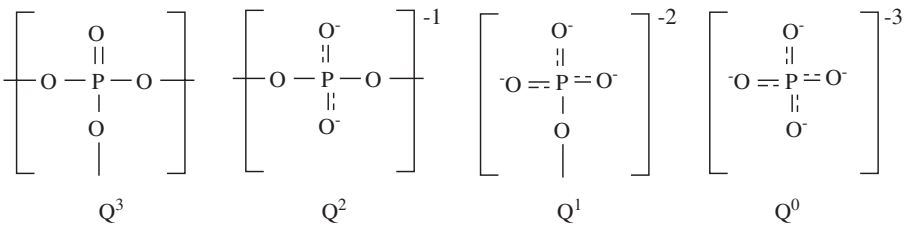

Fig. 3. Naming scheme of the phosphate anion tetrahedra in phosphate glasses.

is the number of bridging oxygen present [19]. As these building blocks can form different types of networks, they are identified using the oxygen to phosphorous ratio. For example, vitreous phosphate glass has a ratio of exactly 2.5, while ultraphosphate glasses have a ratio that ranges from 2.5 to 3.0. It is common practice to use NMR spectroscopy, high-performance liquid chromatography, and Raman spectroscopy to identify the fraction of each phosphate anion tetrahedra present in a specific glass composition, thereby giving structural information about the glass [19,23–25]. It is also possible to obtain additional structural information using X-ray or neutron scattering techniques [26,27]. Researchers have used these diffraction techniques to determine the average bond length of the metal cation–oxygen bond and the phosphorus–oxygen bond [19]. Surprisingly, the phosphorus–oxygen bond length is actually affected by the metal cation present in the glass. The cation plays a large role in determining both the structure of the phosphate glass as well as its thermal properties. For example, lead pyrophosphate glasses have T_gs around 390 °C, while zinc alkali phosphate glasses display T_gs that range from 270 to 330 °C, as well as favorable rheological characteristics in the liquid state [28–30]. Phosphate glasses also display a wide range of desirable properties such as low preparation temperatures, chemical durability, high thermal expansion, good electrical conductivity, optical clarity, UV transparency, and biocompatibility [27]. These properties have led to a variety of uses for phosphate glasses in a number of applications such as nuclear waste storage media, glass to metal seals, solid electrolytes, and bioceramics [27].

The glass composition of most interest to the long-range research program described in this review article is tin fluorophosphates (TFP) glasses. (Note that other Pglass compositions are available.) TFP glass was discovered and patented by Tick and Sanford in 1982 [31]. This Pglass composition resulted in an optically clear glass that, unlike other traditional Pglass compositions, displayed excellent water resistance. These properties have led to a range of possible applications for these glasses including many optical uses [32]. A second patent was issued 1 year later to Paul Tick, which described the use of TFP glass as a supporting matrix for light-responsive polycyclic aromatic hydrocarbons [33]. One of the claims in the patent just mentioned was based on the discovery of a family of materials which contained a significant portion of organic material. Tick continued his work on TFP and lead-TFP glasses and determined the properties and a tentative network repeat unit for these glasses [34]. Tick's prior work was further supported and refined by Xu and Day and the repeat unit of the TFP glass network, which is shown below, was elucidated [35,36].

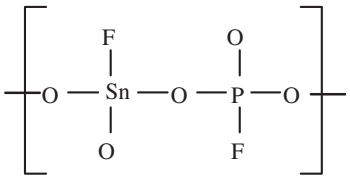

The specific phosphate glass composition of interest to recent research efforts has a molar composition of 50% SnF_2 + 20% SnO + 30% P_2O_5. This results in a Pglass with a T_g of approximately 125 °C and a density of 3.75 g/cm^3. Adalja and Otaigbe [37] have shown that this glass behaves essentially like a Newtonian fluid over a wide range of frequencies and temperatures and its viscosity is strongly temperature dependent, like others have reported for zinc alkali phosphate glass in the liquid state as already mentioned [30]. The rheological behavior combined with the low T_g of this TFP glass composition makes it ideal for use in inorganic/organic hybrid materials.

Due to their low T_g, this phosphate glass composition is liquid over a range of temperatures that includes the melt processing temperature of many different polymers. Therefore, it is possible to blend these inorganic glasses with organic polymeric materials in the liquid state, using conventional polymer processing methodologies, to yield hybrid materials containing Pglass loadings of up to 60% by volume or 90% by weight. Because both the organic polymer and inorganic Pglass are fluid during processing, the morphologies of these materials can be controlled, the interactions between components can be tailored, and the intractable viscosity problem inherent to conventional polymer composites at high solid filler (e.g., borosilicate glass) compositions is circumvented [38–41].

In this review article, we examine the current state of research into these unique phosphate glass/polymer hybrids. While prior work on TFP glass/polymer hybrids has concentrated on non-polar, non-interacting commodity resins or high-end engineering thermoplastics, extending this field to include highly interacting commodity resins, such

as polyamides, new hybrids with very unique and interesting properties can be generated. A brief literature survey will be followed by a discussion of new experimental results on three different representative Pglass/polymer hybrids (i.e., Pglass/LDPE (low-density polyethylene) hybrids, Pglass/polyamide 12 hybrids, and Pglass/polyamide 6 hybrids). The goal is to highlight the effect of interaction between the inorganic phosphate glass and the organic polymer on the hybrid's properties. Although significant advances in understanding the behavior of these interesting materials have been realized, many unanswered questions remain. These questions are discussed to help guide future research directions. It is hoped that this article will provide a basis for understanding the fundamental effects of composition, processing parameters, and interaction strength on the structure/property relationships in TFP glass/polymer hybrids. In turn, this understanding can be combined with further systematic studies into novel Pglass/polymer hybrids to generate a better fundamental understanding of their behavior, thereby leading to a new class of industrially useful materials from already existing materials.

2. Survey of current literature on phosphate glass/polymer hybrid materials

Because phosphate glass/polymer hybrid materials represent a relatively new and emerging class of new advanced materials, only a handful of systems have been investigated and reported in the literature. Hybrids of various special Pglass compositions and LDPE, polypropylene (PP), polystyrene (PS), polyphenylene sulfide (PPS), polyetherimide (PEI), polyarylsulfone, poly(ether ether ketone), and a liquid crystalline polymer (LCP) have been reported [20,42–44]. A large number of the previous studies just mentioned concentrated on characterizing and analyzing the hybrid rheology at very high Pglass concentrations to accelerate efforts to melt process the hybrid components using conventional polymer processing methods. Like others have reported for classical polymer blends, it is worthy to note that understanding and controlling the rheological properties of the hybrids are crucial in determining the final morphology of the material as well as its processability.

A number of researchers used zinc alkali phosphate glasses (T_gs $>272\,^{\circ}C$) as the Pglass for hybrid systems involving engineering thermoplastics with high melt flow temperatures [42–44]. For example, it has been shown for a Xydar® LCP [poly (*p*-hydroxybenzoic acid-*co*-bisphenol terephthalate)] hybrid system that the viscosity of the system, as compared to that of the pure LCP, increased only slightly at low shear rates and was unchanged at high shear rates [43]. It was also demonstrated that a variety of morphologies, such as droplets and fibrils, could be achieved as shown in Fig. 4 [42,43]. The rheology of Pglass/PEI hybrids was qualitatively examined through evaluation of its processing behavior by Young and co-workers [44]. They found that the Pglass modified the flow behavior of the PEI and enhanced the formability of the hybrid and its resultant properties [44]. Otaigbe and co-workers examined zinc alkali Pglass/LCP hybrids and zinc alkali/poly(ether ether ketone) hybrids. They found that the thermorheological stability of the material depended on the polymer matrix and that the resultant morphologies and properties depended on the processing history [42]. Table 1 summarizes selected properties (measured according to standard ASTM methods) of these novel hybrid materials along with that of existing materials such as the pure hybrid components, commodity plastics and polymer/clay nanocomposites. Note that the values shown in Table 1 for the commodity plastics depend on molecular weight and processing conditions. It is worthy to note that the flexural modulus of the hybrid composition shown increases dramatically with increasing volume fraction of Pglass ($\geqslant 50\%$) and with use of expensive high-temperature polymers such as poly (ether ether ketone) and poly(ether sulfone) by a factor of about 10 relative to that of the pure polymers and polymer/clay nanocomposites [43], illustrating the potential of the Pglass/polymer hybrids.

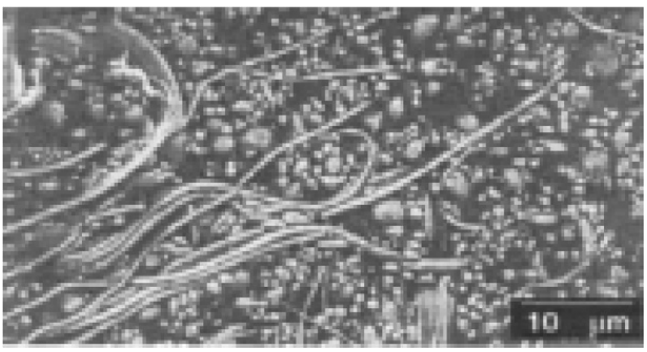

Fig. 4. Examples of the unique morphologies generated in zinc Pglass/Xydar® LCP hybrids [43]. (Reproduced from Quinn, Frayer and Beall by permission of CRC Press, New York.)

Table 1
Selected material properties of different types of materials

Material	Modulus (GPa)	Density (g/cm^3)	Refs.
Pglass/LDPE hybrid (50 vol.% Pglass)	~11	2.33	[45a] (this work)
Polymer/clay nanocomposites	0.5–1.0	N/A	[9]
Phosphate glass (Pglass)	~40	3.75	[21]
Low-density polyethylene (LDPE)	0.14–0.31	0.92	[45b]
Commodity plastics	<0.50	0.91–1.05	[45b]

The effect of TFP glass on Pglass/LDPE hybrid rheology has been reported elsewhere [37,38,45–48]. Because TFP glass has a T_g of about 125 °C, they can be easily mixed in the liquid state with commodity plastics such as polyethylene. Adalja et al. [37,38,45] studied TFP/LDPE hybrid rheology and found that while the time–temperature superposition principle applied to these materials, the Pglass induced strong shear thinning behavior and reduced creep strain in the solid state [37,38,45]. They also successfully treated the Pglass with silane coupling agents, which resulted in an increase of the complex viscosity [38,45]. Guschl et al. [46–48] studied hybrids of TFP glasses and LDPE, PS, and PP in the liquid state. They used torque rheometry to reveal a trend towards linear additivity for TFP glass/PS hybrids, and used small amplitude oscillatory shear measurements to determine the phase inversion point for this hybrid system [47]. In addition, Guschl et al. [46] also measured and reported the interfacial tension between TFP glass and LDPE, PS, and PP. They compared pendant drop measurements to the Palierne and Choi and Schowalter theoretical emulsion models [49,50]. These models fit the TFP glass/PS and TFP glass/PP hybrids with Pglass loadings up to 10 vol%. However the models were found to be inadequate for hybrids containing more than 30 vol% Pglass and for the LDPE hybrids at all TFP glass concentrations studied. Further, Guschl et al. [48] also examined steady shear and transient rheology of a ternary Pglass/PS/LDPE hybrid system. The liquid rheological properties of the ternary hybrid depended strongly on Pglass concentration with hybrids at moderate Pglass loadings (>30 vol%), displaying a flow behavior similar to that of liquid crystal polymers [48].

Other researchers have studied the interfacial tension, crystallization kinetics, and mechanical properties of these unique hybrid materials. For example, Carre [51] reported that the addition of tin oxide to zinc phosphate glasses dramatically reduced the interfacial free energy between the glass and polyethersulfone using a modified drop shape method. The crystallization behavior of TFP glass/LDPE and TFP glass/PP hybrids has also been studied [32,52,53]. It has been found that the addition of Pglass to any polymeric matrix consistently reduces the overall crystallinity in the system. However, the effect of Pglass on the crystallization kinetics of the organic polymer is dependent on both the polymer matrix and Pglass concentration. Further studies into the crystallization behavior of these materials using NMR spectroscopy revealed that TFP glass does not affect the crystalline structure of LDPE, but the glass itself undergoes significant structural changes upon hybrid formation [32]. The mechanical properties of various hybrids have also been reported [43,44,53,54]. It has been shown that certain Pglass hybrids exhibit higher Young's modulus and flexural strength values than equivalently filled conventional composites [43,44,54]. These prior studies reported in the literature highlight the unique nature of Pglass/polymer hybrids. While much insight into the behavior of these materials was gained from these prior studies, more work needs to be done before Pglass/polymer hybrids can achieve their full technological potential. It is hoped that the current article will provide guidelines for future research studies on these truly intriguing materials.

3. Preparation of TFP glass/polymer hybrids

The low T_g Pglass used in the studies described in the next section has a molar composition of 50% SnF_2 + 20% SnO + 30% P_2O_5. This results in a glass with a density of 3.75 g/cm^3 and a T_g of 125.7 °C. The glass was synthesized in the author's laboratory using procedures reported elsewhere [37]. The tin fluoride and tin oxide were supplied by Cerac Inc. and the ammonium phosphate was supplied by Sigma-Aldrich. The LDPE type 1023 used was supplied by Huntsman Chemical Corporation, the polyamide 12 (Vestamid® L1700) was supplied by Creanova Inc., and the polyamide 6 used was Capron 8270 HS supplied by Allied Signal. The hybrids were prepared using a Thermo-Haake

Polydrive® Melt Mixer equipped with roller blades. LDPE hybrids containing the desired amount of Pglass were mixed at 200 °C, while the polyamide 12 and the polyamide 6 were mixed at 220 and 250 °C, respectively. Prior to melt-mixing, the polymer and the Pglass are dried in a vacuum oven. The Polydrive® mixer was preheated to the desired mixing temperature for at least 20 min before mixing in order to ensure that the instrument had reached thermal equilibrium. Before any of the hybrid components are added to the mixer, the instrument is calibrated at the appropriate mixing speed. First, the polymer is added to the Polydrive® mixing bowl and allowed to mix for some time in order to yield a homogeneous melt. The Pglass is subsequently added in the required amounts to the mixer and allowed to mix for additional period of time. The addition of the hybrid component materials to the Polydrive® can be automatically monitored in a graph of torque versus time as shown in Fig. 5. The first spike in torque is the addition of the polymer, in this case polyamide 6, and the precipitous drop in the torque around 300 s corresponds to the addition of the Pglass. The melt-mixed hybrid materials were collected in "chunks" from the Polydrive®. Prior to further processing, the materials were dried in a vacuum oven. The "chunks" were then formed into a variety of shapes for testing using either a Tetrahedron® compression molder or a DACA Microinjector® equipped with the appropriate mold at the same temperature used during melt-mixing.

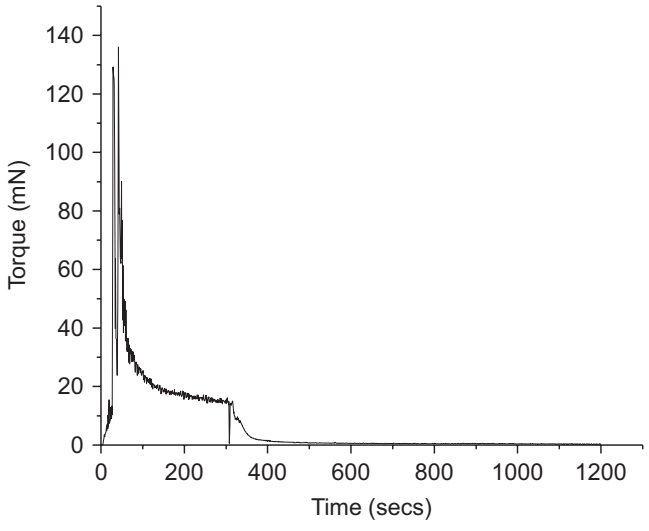

Fig. 5. Typical torque versus time graphs recorded during the mixing process for Pglass/polyamide 6 hybrids.

4. New experimental results

4.1. Pglass/LDPE hybrids

LDPE is a non-polar polymer that displays a high interfacial tension when it is combined with Pglass [46]. The combination of these two non-interacting components to form a Pglass/LDPE hybrid yields a material with interesting morphologies and unique properties described later. It is important to understand this material's elongational flow behavior if it is to become industrially useful. Elongational flow is an important component of many processing techniques [55,56]. A deformable particle that experiences simple shear flow will deform only slightly and will rotate in the flow field at a rotation rate equal to half the shear rate. On the other hand, a deformable particle undergoing extensional flow will experience no rotation, but a lot of deformation along the flow axis. Upon the cessation of flow, the deformed particle will experience compression along the flow axis as the deformed particle tries to return to its original shape [57]. Many polymeric materials that undergo extensional flow exhibit a dramatic increase in viscosity at high strains which is referred to as strain hardening. The stain hardening phenomenon is related to the uncoiling of polymer chains. This coil-stretch transition results in very long, aligned particles [57]. The strain hardening behavior of a polymeric material or blend plays a large role in processing methods like extrusion, blow molding, and thermoforming. Therefore, it is important to study the behavior of materials under elongational flow.

Studies of elongational flow of polymer melts began in the 1970s and continue today [58]. One of the earliest methods of measuring elongational viscosity was the rotary clamp technique. This technique involves large, homogeneous elongations in the sample and the force on the clamps is used to get a reliable stress measurement [58]. The major drawback of this technique was the need to use a supporting liquid for the sample, which limited the temperature range of the instrument. Meissner *et al* .[58] developed a relatively new rheometer which eliminated the problem just mentioned by supporting the sample on a cushion of nitrogen gas. This rheometer has proven to be both versatile and accurate [59,60].

It is important to understand the shear rheological behavior of a material prior to elongational flow investigations. Additionally, it is well known that shear rheological properties are important in under-

standing the morphology development of the current hybrids [45a,61]. Therefore, small amplitude oscillatory shear measurements were performed at 180 °C on the Pglass/LDPE hybrids prior to elongational viscosity measurements [41]. Note that both the shear and elongational measurements just mentioned were performed in the liquid state. A strain amplitude sweep was performed on the hybrids to determine the linear viscoelastic region of the hybrids. For frequency sweeps of the hybrids, a linear strain of 10% was used for hybrids containing ⩽20% by volume Pglass. A linear strain of 1% was used for the pure Pglass and hybrid compositions containing between 30% and 50% by volume Pglass. The results of the small amplitude oscillatory shear measurements are shown in Fig. 6. As Pglass is added to the system, the viscosity increases. Additionally, hybrids containing ⩽30% Pglass display a Newtonian plateau at low frequencies and become shear-thinning at the high frequencies. The hybrids with high Pglass concentrations show strong shear-thinning behavior over the whole range of frequencies investigated, which is consistent with results reported by Adalja et al. [45a]. The pure Pglass liquid is approximately Newtonian over the 0.1–100 rad/s experimental range of frequencies. A small increase in the Pglass viscosity at high frequencies was observed and is attributed to shear-induced crystallization which has been observed previously for these types of glasses [37]. The shear-induced crystallization of the Pglass is also evidenced by an increase in storage modulus at a high frequency. The Pglass also displays a small rise in complex viscosity at the very low frequencies (i.e., $\omega < 0.1$ rad/s). This rise in complex viscosity was unaffected by annealing and found to be a

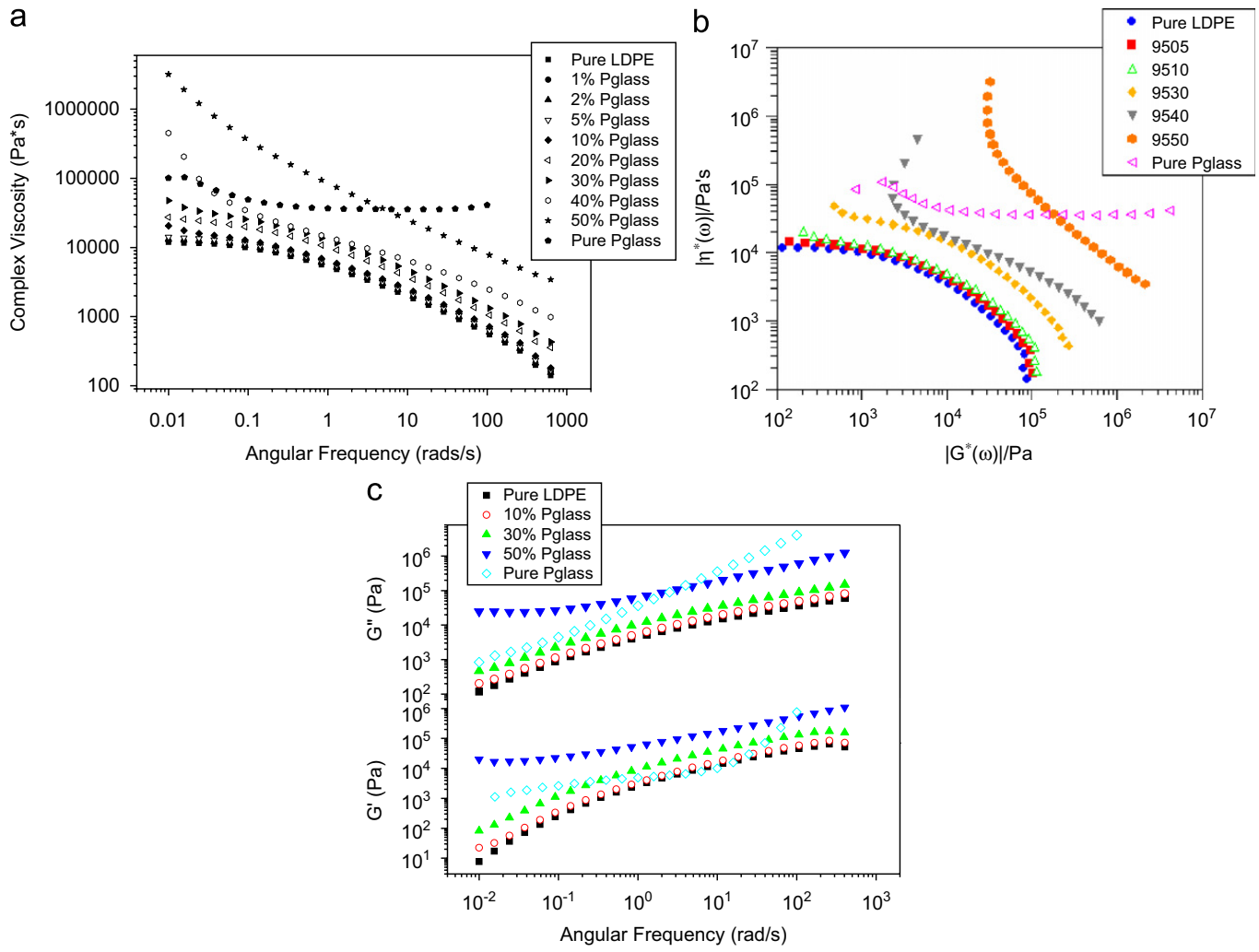

Fig. 6. (a) Frequency dependence of complex viscosity of Pglass/LDPE hybrids and pure components at 180 °C, (b) plots of complex viscosity, $\eta^*(\omega)$, versus complex modulus, $G^*(\omega)$, for the hybrids and (c) frequency dependence of the storage and loss modulus of selected hybrids and the pure components. Other hybrid compositions are not shown for clarity.

consistent, reproducible feature of the material. It is believed that the complex viscosity increase at low frequencies is most likely due to some structural rearrangement of the Pglass network structure [20,62].

Fig. 6b displays logarithmic plots of the frequency dependence of the complex viscosity, $\eta*(\omega)$, versus the frequency dependence of the complex modulus, $G^*(\omega)$, for the Pglass/LDPE hybrids and their pure components. Such plots are useful for observing yield stress behavior from experimentally determined viscoelastic material functions. A sharp upturn in $\eta^*(\omega)$ at low $G^*(\omega)$ indicates the existence of a yield stress. Note that similar plots of $\eta^*(\omega)$ versus $G^*(\omega)$ and of other viscoelastic functions such as $G'(\omega)$ and $G''(\omega)$ have been used by others in the literature for the same purpose as in this study or as a criterion for rheological compatibility of polymer blends [2,63–65]. It is clearly evident from Fig. 6b that the Pglass concentration has a strong influence on the hybrid complex viscosity especially at Pglass concentrations >30 vol%. At these Pglass concentrations, the hybrids do not show a Newtonian region within the experimental frequency range that would have manifested itself by a constant $\eta^*(\omega)$ at low $G^*(\omega)$. The sharp upturn of $\eta^*(\omega)$ on the low $G^*(\omega)$ side (i.e., $\eta^*(\omega)$ increases as $G^*(\omega)$ decreases) exhibited by the hybrids with Pglass concentrations >30 vol% suggests that these hybrid compositions have a yield stress for viscous flow due to the formation of a co-continuous (interpenetrating network) structure (discussed later) in the hybrids. In contrast to the hybrid compositions just mentioned, the hybrids containing Pglass concentrations <30 vol% tend to approach constant $\eta^*(\omega)$ at low $G^*(\omega)$, implying that these hybrids approach Newtonian behavior at low frequencies with no evidence of the possible existence of a yield stress. A close examination of Fig. 6 would indicate a hybrid phase inversion point (or critical Pglass volume content for phase inversion) occurring between 40 and 50 Pglass vol %. This phase inversion point is consistent with a change of deformable droplet to co-continuous morphology in the hybrids and with the previously reported phase behavior of the hybrid system [47].

It is noteworthy that the hybrid composition-independent behavior of $\eta^*(\omega)$ at low Pglass concentrations of <30 vol% and the significant reduction in viscosity at high frequencies (i.e., strong shear thinning behavior) observed for all hybrid compositions studied signifies relative ease of processing of the hybrids and facile manipulation of their morphology via conventional processing methods such as extrusion and injection molding.

The Cross equation (1) could be successfully applied to hybrid compositions with less than 40% Pglass by volume with R^2 values $\geqslant 0.98$ (Fig. 7), according to the following equation:

$$\eta^* = \frac{\eta_0}{1 + (\omega/\omega_c)^{\beta}}, \tag{1}$$

where η^* is the complex viscosity, η_0 is the zero shear viscosity, ω is frequency, and ω_c and β are fitting parameters. The fit parameters are shown in Table 2. The higher Pglass compositions (i.e., 40 and 50 vol%) could not be modeled due to the yield stress behavior at low frequencies already discussed.

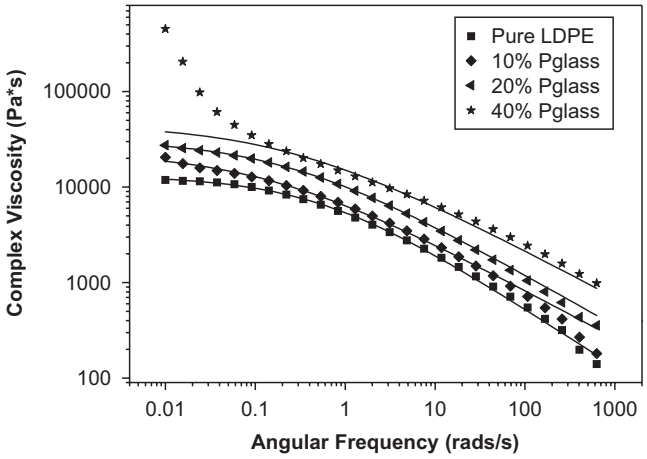

Fig. 7. Cross model fit (solid lines) for typical Pglass/LDPE hybrids.

Table 2
Parameters (ω_c and β) of the Cross model fits to the experimental complex viscosity data of the Pglass/LDPE hybrids

Pglass concentration (vol.%)	Zero shear viscosity (Pa s)	ω_c	β
0	13,119	0.557	0.613
1	13,901	0.525	0.601
2	14,419	0.493	0.593
5	15,925	0.430	0.581
10	23,452	0.144	0.507
20	31,695	0.241	0.539
30	55,920	0.078	0.500
40	Not applicable	Not applicable	Not applicable
50	Not applicable	Not applicable	Not applicable

The observed increase in viscosity at low frequencies is attributed to the formation of a co-continuous interpenetrating network structure. Although the interfacial interaction between the Pglass and the LDPE phases is quite low due to the high interfacial tension between the components, these interactions are playing a large role in the hybrids which display a co-continuous type morphology, thereby leading to the increase in complex viscosity at low frequency [46].

The shear rheological behavior of the Pglass/LDPE hybrids revealed a strong dependence of viscosity on morphology. Investigations into the elongational flow will provide more information into the relationship between rheology and morphology, as well as flow induced structure. Elongational viscosity measurements of the Pglass/LDPE hybrids were performed at 180 °C (liquid state) and at a constant strain rate of $1.0\,s^{-1}$. Lower strain rates were evaluated, but the hybrids containing more than 5% Pglass would sag onto the metal frit of the sample supporting system. The results of the samples tested at $1.0\,s^{-1}$ are shown in Fig. 8. Each of these samples had the true strain rate of the test determined by particle tracking, and the viscosity curves shown in Fig. 8 reflect the true strain rate. The results in Fig. 8 were also normalized to permit valid comparison with the previously discussed oscillatory shear measurements. The normalization was performed using an in-house computer program written by Schweizer for automatic data analysis. The program utilizes Trouton's ratio to normalize the elongational data with the zero shear viscosity for accurate comparison of data. This normalization procedure does not attempt to model the data, it only aids in the comparison of the data. It is clearly evident in Fig. 8 that all of the curves display a shape typical of strain hardening polymers, except for the 50% Pglass/LDPE hybrid (not shown). The odd shape of the 50% Pglass/LDPE curve (not shown) is most likely due to the uneven deformation that characterized all of the tests of the 50% Pglass/LDPE hybrid material. The inhomogeneous deformation of the 50% Pglass hybrid results in unreliable data and, therefore, this composition is not included in any discussion so as not to lead to incorrect conclusions. In Fig. 9, the ratio of maximum viscosity to zero shear viscosity obtained during the elongational viscosity tests, which is an indication of the strain hardening character of a material, is plotted as a function of hybrid composition. It is easily seen from this figure that small concentrations of Pglass ($\leqslant$2% Pglass) actually increase the strain hardening behavior of the LDPE; the intermediate concentrations of Pglass (i.e., 5–10%) display a slight reduction of the strain hardening character, and the high Pglass concentrations ($>$10%) dramatically reduce the strain hardening of the LDPE. The pure Pglass liquid should show insignificant strain hardening as it has been previously shown that the Pglass used in this study is essentially a Newtonian fluid under the reported test conditions. A pure Newtonian fluid will display

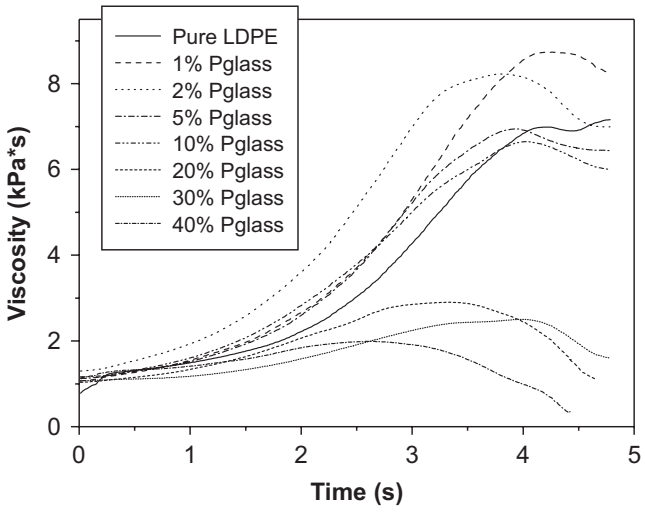

Fig. 8. Elongational viscosity at a strain rate of $1.0\,s^{-1}$ for the Pglass/LDPE hybrids.

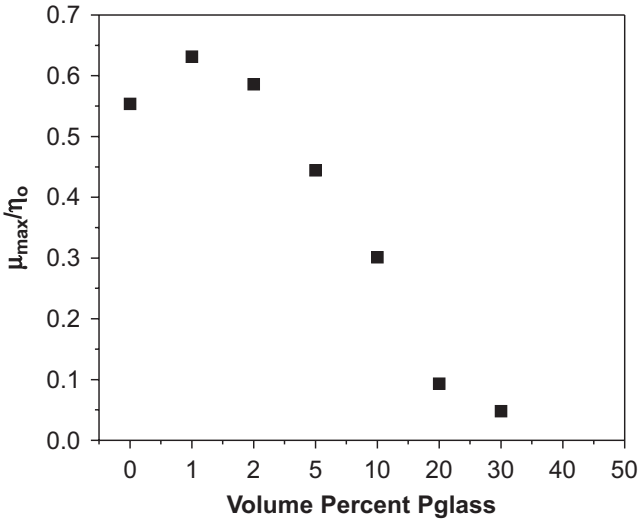

Fig. 9. Ratio of maximum elongational viscosity (μ_{max}) to zero shear viscosity (η_0) of Pglass/LDPE hybrids as a function of hybrid composition. Note that data for the 40% and 50% hybrid are not included in this figure because they show an upturn in viscosity at low frequencies.

little strain hardening, as it is typically a viscoelastic effect. Additionally, when a non-Newtonian fluid, such as LDPE, is diluted by a Newtonian fluid, the strain hardening behavior should decrease. It has been shown in the literature that the addition of solid, non-deformable glass particles to LDPE yields a decrease in the strain hardening character of the pure LDPE [66]. A similar decrease of the strain hardening character was also observed as rigid glass fibers were added to polyethylene and PS melts [67]. Chan and co-workers used Goddard's theory [68] to qualitatively explain this behavior and stated that in elongational flow of oriented glass fibers, shear motions are created between the fibers. If the fibers are contained in a non-Newtonian matrix, the shear viscosity will be much less than the zero-shear viscosity, resulting in a reduction of the elongational viscosity [67]. However, this explanation is only valid for non-deformable particles. Other researchers have shown that deformable, viscoelastic fibers typically lead to an increase in elongational viscosity, while deformable spheres have little impact on the elongational viscosity [69]. It has also been shown that the addition of a linear polyethylene (HDPE or LLDPE) to LDPE causes a decrease in strain hardening because the linear polyethylene is acting as a non-strain hardening diluent [70,71]. From the preceding discussion, it is reasonable to ascribe the dramatic reduction in the hybrid elongational viscosity at Pglass concentrations $>10\%$ to disentanglement and/or scission of the LDPE chains caused by the plausible physicochemical interaction of the Newtonian Pglass. This is a matter for further investigation.

While the hybrids with high Pglass concentrations ($>10\%$) display behavior that is consistent with that reported in the literature, the low Pglass concentrations display relatively anomalous behavior. However, the observed behavior can be explained by considering the morphologies of stretched and unstretched samples (Fig. 10). Column I is the samples prior to stretching and Column II is the samples after stretching. Although the Pglass is a liquid at the test temperature, the Pglass particles in the 1% and 2% hybrid samples do not deform. It is only when the Pglass concentration reaches 5% by volume that the particles begin to undergo deformation. The mechanism of the observed increase in elongational viscosity at very low Pglass concentrations is presently unclear, and needs to be further explored in future studies. This hypothesis needs to be further tested in future studies.

The observed hybrid morphologies can be further understood by examining the capillary number of the hybrid materials. In shear flow fields, the capillary number is defined according to the following equation:

$$Ca = \frac{\eta_m \dot{\gamma} d_n}{2\Gamma_{12}}, \tag{2}$$

where η_m is the shear viscosity of the matrix, $\dot{\gamma}$ is the shear rate, d_n is the droplet diameter, and Γ_{12} is the interfacial tension between the matrix and the dispersed phase. When the capillary number of a material exceeds some critical value, Ca_{crit}, a droplet will change its shape and eventually breakup. However, this breakup is not instantaneous, and researchers have been able to induce a fine, fibrillar morphology in some polymer blend systems [56,59]. During deformation, a material that exceeds the value $2 \times Ca_{\text{crit}}$, will undergo a morphological change, where droplets deform into a fibril morphology [72]. Münstedt et al. [72] defined a capillary number for materials undergoing elongational flow, Ca_E according to the following equation: .

$$Ca_E = \frac{\eta^+_{E,m} \dot{\varepsilon} d_n}{2\Gamma_{12}}. \tag{3}$$

The variables in Eq. (3) are defined similarly to those in Eq. (2). However, there are some notable differences. The shear viscosity of the matrix and shear rate in Eq. (2) has been replaced by the elongational viscosity of the matrix, $\eta^+_{E,m}$, and the strain rate, $\dot{\varepsilon}$. The capillary number for Pglass/LDPE hybrids that displayed droplet type morphology in the unstretched state ($<40\%$ Pglass by volume) was calculated. The interfacial tension of LDPE and Pglass was previously determined at different temperatures by Guschl and Otaigbe [46]. Since they did not determine the interfacial tension at the temperature used for testing in the current work described in this article, a simple weighted average was taken and a value of 54.92 mN/m was used for the calculations. The average droplet diameter was measured for each hybrid and the results are displayed in Table 3. The elongational viscosity of the matrix was taken as the maximum elongational viscosity for pure LDPE shown earlier in Fig. 9. The calculated Ca_E for the hybrids is shown in Table 4. An approximation of Ca_{crit} for the hybrid systems can be found. As the 10% Pglass hybrid is the first composition to display fibril-like morphologies, it can be assumed that the elongational capillary number for this composition is

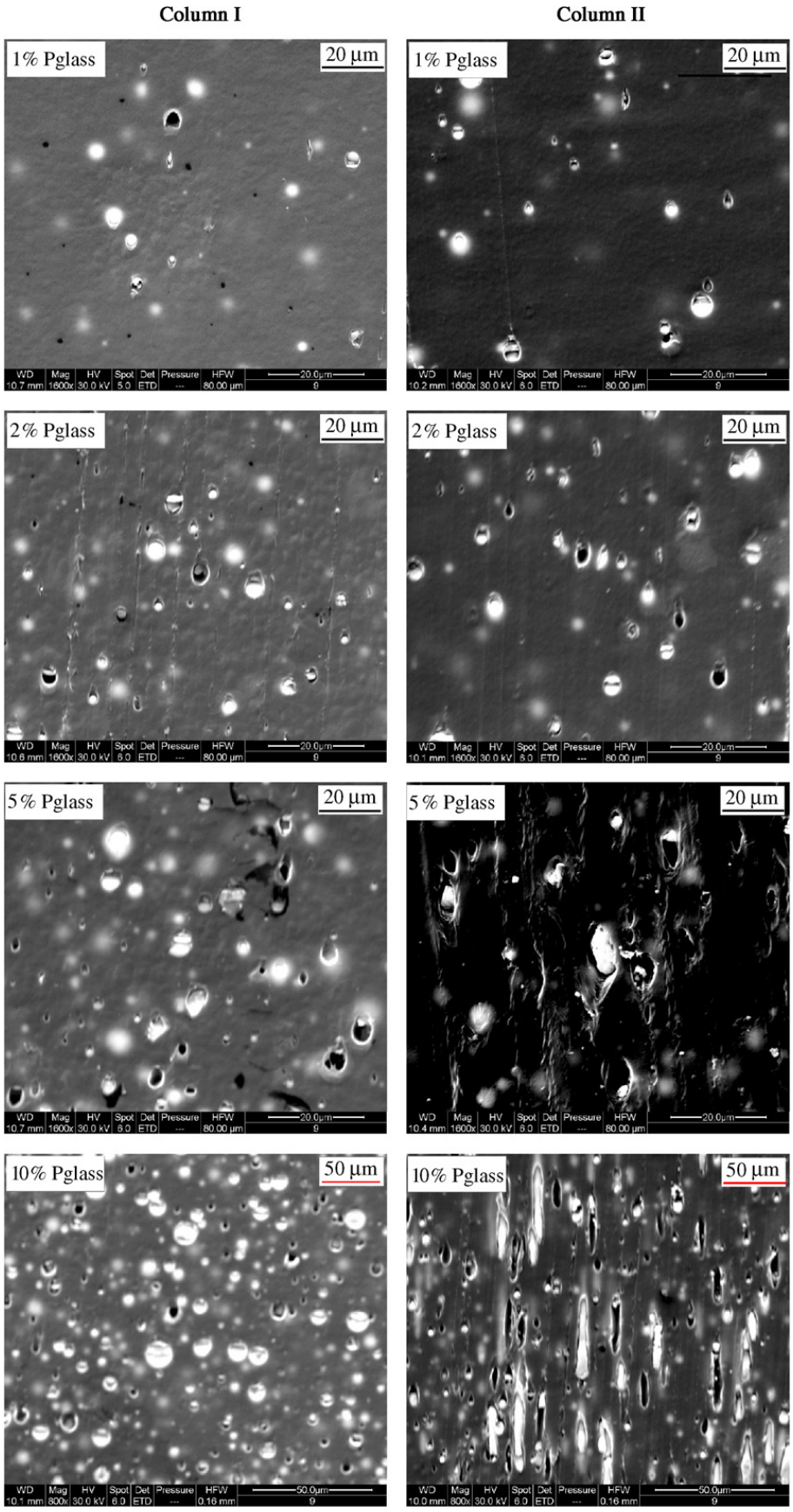

Fig. 10. (a, b) SEM micrographs of Pglass/LDPE hybrids before melt elongation (column I) and after melt elongation (column II).

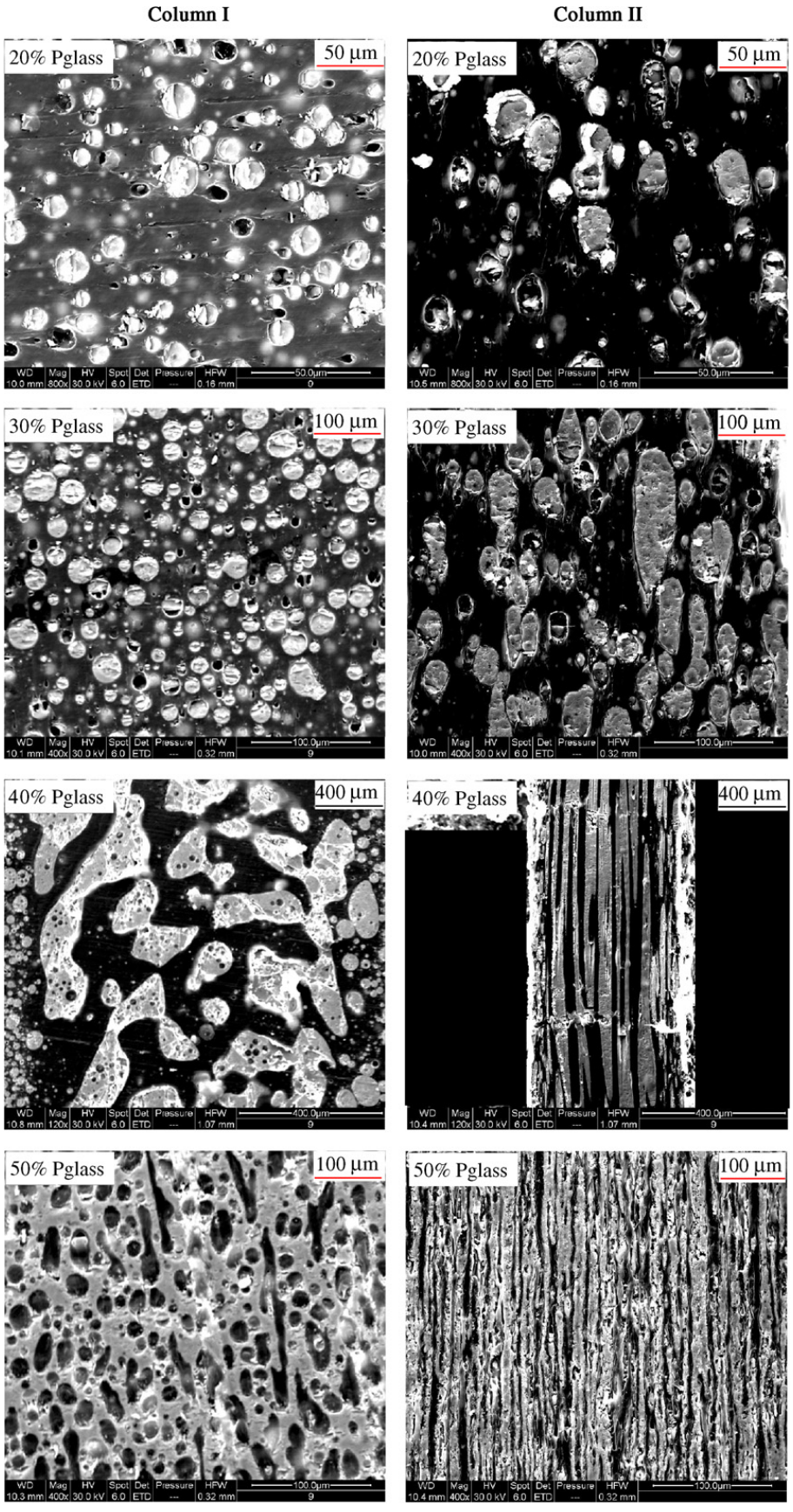

Fig. 10. (*Continued*)

Table 3
Particle size of Pglass/LDPE hybrids

Pglass concentration (vol.%)	Size (μm)
1	2.71 ± 0.99
2	2.27 ± 0.93
5	3.89 ± 1.11
10	6.60 ± 2.40
20	8.68 ± 2.72
30	12.22 ± 3.94
40	Not applicable
50	Not applicable

Table 4
Elongational capillary number for Pglass/LDPE hybrids

Pglass concentration (vol.%)	Elongational capillary number
0	Not applicable
1	0.182
2	0.153
5	0.262
10	0.444
20	0.584
30	0.822
40	Not applicable
50	Not applicable

closest to $2 \times Ca_{crit}$. This gives an approximate value of Ca_{crit} of 0.22. Considering that the variation in capillary number for the Pglass/LDPE hybrids is solely due to changes in Pglass droplet size, these results can provide a guide for morphological control and rational design of Pglass/LDPE hybrid systems.

Elongational flow provides a facile route to creating new and interesting morphologies for Pglass/polymer hybrids. Investigations into the elongational viscosity can also generate fundamental insights into the parameters controlling morphological development for Pglass/polymer hybrids. Another interesting effect of uniaxial elongation of a polymeric material is the alignment of polymer chains during deformation. This alignment causes a general increase in crystallinity of the stretched sample as compared to an unstretched sample [73–76]. The Pglass/polymer hybrids of this study consistently show a decrease in polymer crystallinity as the amount of Pglass in the system is increased [52,53]. The exact mechanism of this phenomenon is presently unknown, but is considered to be a unique feature of these interesting hybrid systems. The possibility of increasing the crystallinity through carefully controlled processing conditions would lead to great improvements in overall material properties. Additionally, it would provide yet another route to the rational control of the morphology, and therefore the properties of these unique systems.

The percent crystallinity of the materials was estimated using a slightly modified equation with respect to that used for pure polymers:

$$X_c = \frac{(\omega^* \Delta H_{obs})}{\Delta H_f^o}. \quad (4)$$

In this equation, ΔH_{obs} is the heat of fusion observed in the DSC experiment, ΔH_f^o is the standard heat of fusion of a 100% crystalline LDPE, and ω is the weight percent of LDPE that is in the hybrid. The ω term of this equation was added to account for the fact that LDPE is the only crystallizable component of the hybrid. The results of these experiments are shown in Fig. 11. Clearly, the uniaxial elongation results in dramatic increases of crystallinity. The stretched 10% Pglass/LDPE hybrid has a percent crystallinity that is only 5% less than the unstretched pure LDPE. The difference in percent crystallinity of stretched and unstretched samples decreases as the amount of Pglass is increased. This is most likely due to the small amount of crystallizable polymer present in the system. However, the stretched samples consistently have a higher percent crystallinity than the unstretched samples over the Pglass concentration range studied.

4.2. Pglass/polyamide 12 hybrids

While Pglass/LDPE hybrids display interesting properties and unique morphologies, new hybrid materials with enhanced interactions between the hybrid components should yield materials with vastly different properties, thereby opening up entirely new fields of study and application for Pglass/polymer hybrids. By combining Pglass with highly interacting commodity resins, such as polyamides, improved interactions between the Pglass and the polymer matrix can be achieved. This is due to the expected strong physiochemical interactions between the hybrid components. For example, it has been shown that ammonia will adsorb to the surface of phosphate glasses [77a]. This classical interaction facilitates a high degree of interaction between polyamides and TFP glass, thereby facilitating both

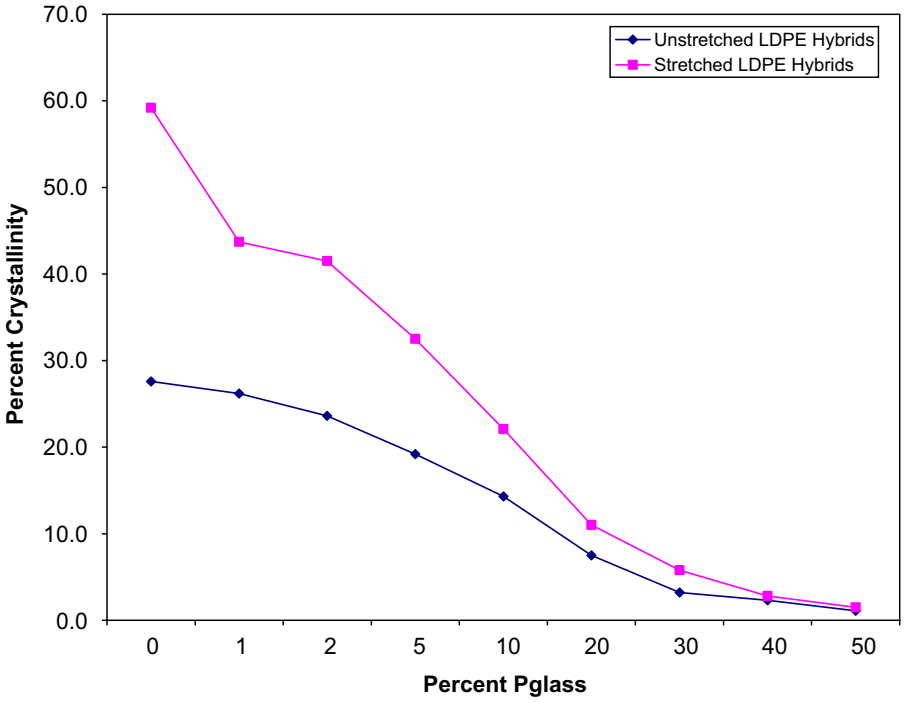

Fig. 11. Percent crystallinity of stretched and unstretched Pglass/LDPE hybrids.

miscibility in the melt and enhanced polymer/glass adhesion in the solid state [40]. This should lead to a hybrid material with good compatibility and interesting melt properties that are typical of either an immiscible or a partially miscible system to an extent that depends on factors such as the processing and testing conditions. The first rheological study of TFP glass/polymer hybrids that display desirable interactions that are beneficial in a number of applications was performed on Pglass/polyamide 12 hybrids [77b].

Fig. 12 shows the frequency dependence of the complex viscosity for the hybrid materials at 190, 220, and 250 °C. Over the whole range of temperatures studied, the pure Pglass behaves like a Newtonian fluid. Due to rheometer limitations, the extremely low viscosity of the pure Pglass at 250 °C causes some scatter in the observed data. At 190 °C, the pure polyamide 12 and all of the hybrids display a long Newtonian region with some slight shear-thinning behavior at high frequency. Additionally, despite the high viscosity of the pure Pglass, at this temperature, hybrids containing $\geqslant$2 vol% Pglass show a dramatic decrease in viscosity, suggesting a plausible constraint release or disruption of the polymer chain entanglements caused by the addition of Pglass. This finding is somewhat similar to the non-Einstein-like decrease in viscosity of PS filled with nanoscale particles reported by Mackay and co-workers [78,79]. This behavior changes as the testing temperature is increased to 220 °C. Hybrids containing $>$5 vol% Pglass begin to show an increase in complex viscosity at low frequencies at this temperature. The increase of the complex viscosity becomes more pronounced as the temperature is further increased. An increase in complex viscosity at low frequencies is often attributed to interfacial affects and yield stress behavior [2,3,80]. Above a critical composition of 2 vol% Pglass, a dramatic change in the interfacial characteristics of the hybrid occurs at elevated temperatures.

The rise in the complex viscosity at low frequencies shown for the 5 and 10 vol% Pglass hybrids has been related to the appearance of an apparent yield stress in the material [81]. Early attempts to describe a yield stress did not allow any elastic behavior below the yield stress, but this was found to be an over simplification for many material systems [82]. As already mentioned, it has been shown that plotting complex viscosity versus complex modulus indicates an apparent yield stress in a material system by an upturn in the graph at low complex modulus values [2,65]. Fig. 13 displays such plots for the hybrid systems at 190 and 250 °C. At 190 °C, all of the hybrids tend to approach constant $\eta^*(\omega)$

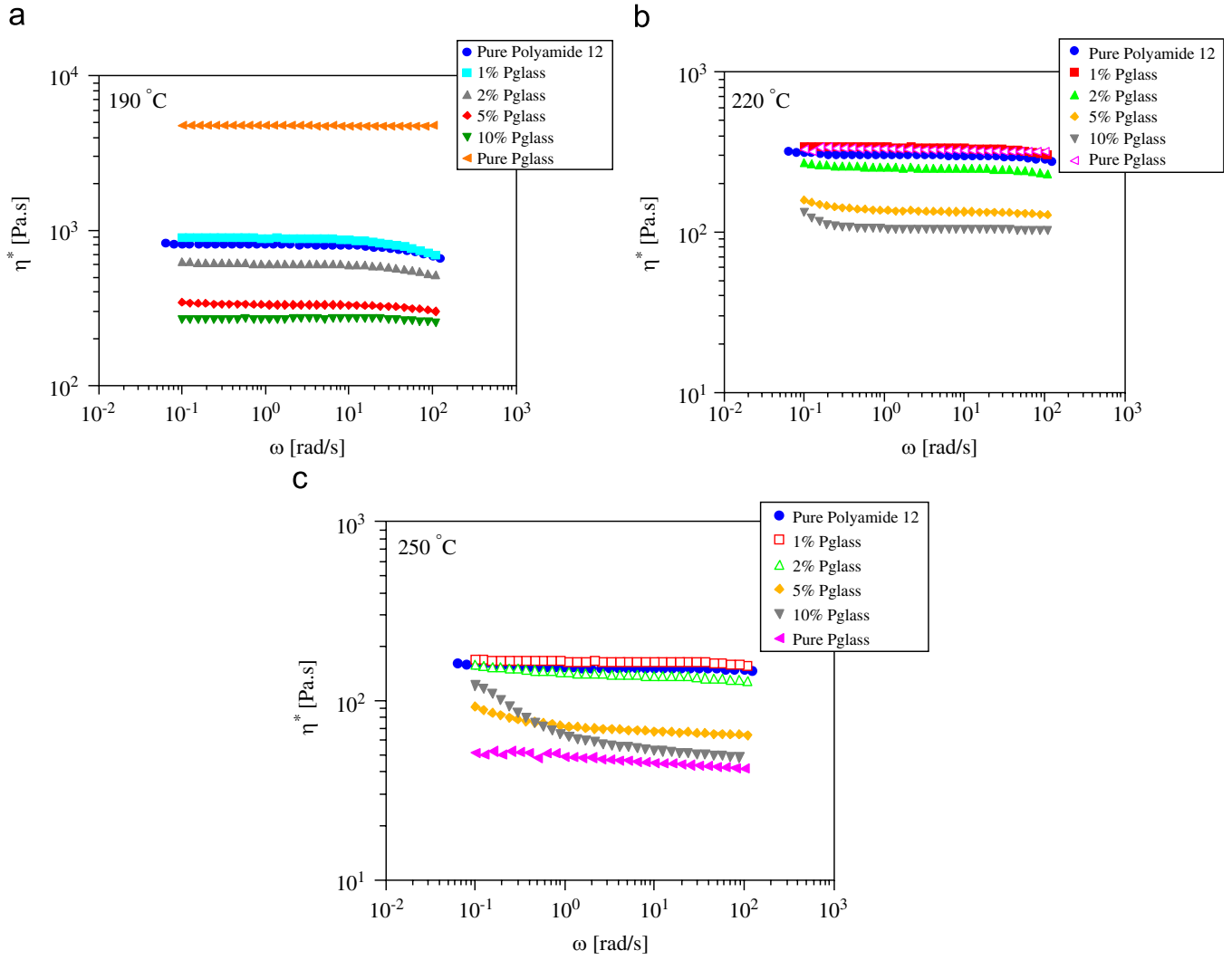

Fig. 12. Frequency dependence of the complex viscosity of polyamide 12 hybrids at (a) 190 °C, (b) 220 °C, and (c) 250 °C.

at low $G^*(\omega)$, implying that these hybrids exhibit Newtonian behavior at low frequencies with no evidence of the possible existence of a yield stress. However, as the temperature is increased, a sharp upturn of the graph is observed for hybrids containing $\geqslant 5$ vol% Pglass, suggesting that these hybrid compositions have a yield stress for viscous flow. Apparent yield stresses have been reported in the literature for some immiscible polymer blends and are usually attributed to strong interactions between the components [2,65,83,84].

Yield stresses have been observed for many different polymer composites and nanocomposite systems at high concentrations of filler, and is typically ascribed to the formation of some filler network or aggregates in the polymer melt [85–87]. Evidence of such a yield stress can be observed by examining the change in slope of the storage or loss modulus as a function of frequency. A reduction of the slope in the terminal region has been observed for polyamide 12/clay nanocomposites and was related to the tendency of the silicate platelets to form a superstructure that displays a yield stress [88]. Fig. 14 depicts the loss modulus of the current hybrid materials at 250 °C and Table 5 shows the slopes of the linear portion of the curves at both 190 and 250 °C. The slopes displayed by the materials at 190 °C are typical for polydisperse polymers and do not indicate any yield stress behavior [88,89]. As the temperature is increased to 250 °C, the hybrids containing $\geqslant 5$ vol% Pglass show a dramatic decrease in the slope, similar to that reported for the polyamide 12/clay nanocomposite. Unlike the silicate nanofillers, the Pglass is fluid at these temperatures. However, it is still likely that the dispersed Pglass can interact with itself to form

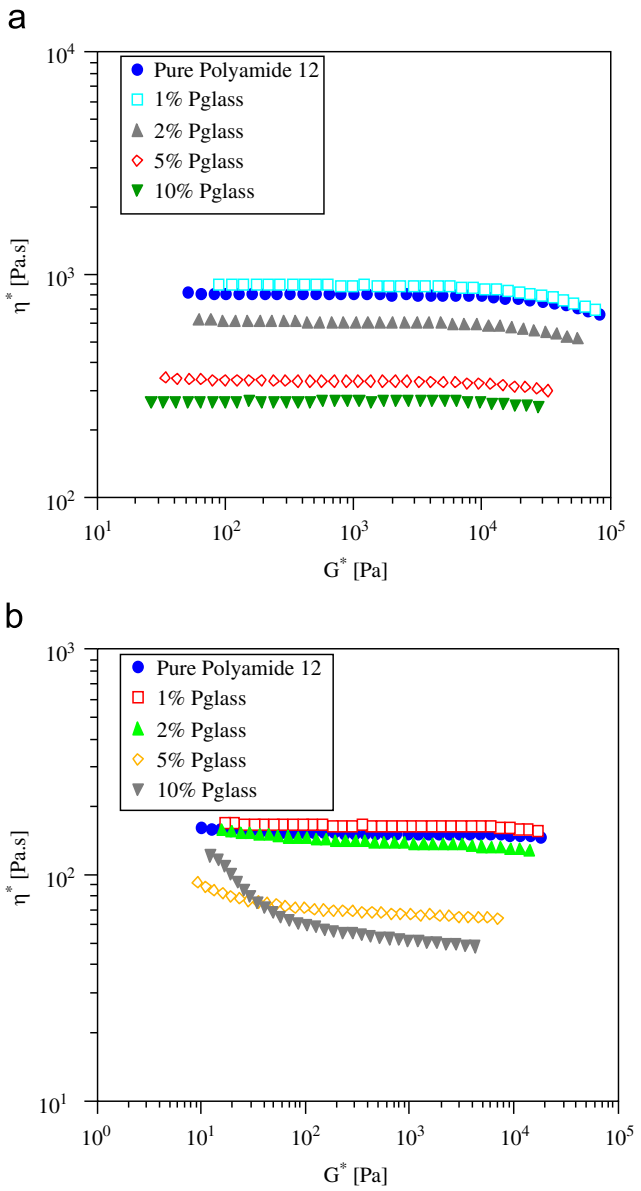

Fig. 13. Complex viscosity versus complex modulus for pure polyamide 12 and studied hybrids at (a) 190 °C and (b) 250 °C.

some kind of superstructure that leads to yield stress behavior as will be shown later. The yield stress behavior observed for the hybrids is consistent with the previously discussed rheological data, indicating that increasing temperature causes a morphological change in the high Pglass concentration hybrids and an associated enhancement of the interactions between the polyamide 12 and the Pglass.

The effect of temperature on the rheological behavior of the hybrids can be further probed using plots of storage modulus (G') versus loss modulus (G''). These plots were first developed by Han and co-workers and have been widely used in the literature to investigate the compatibility, morphological

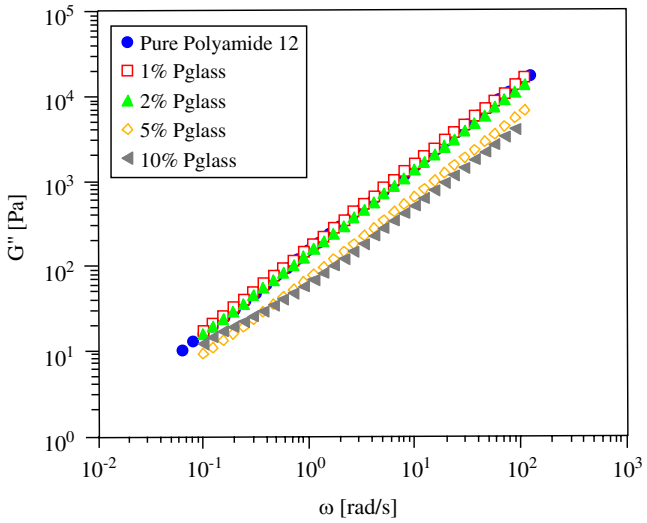

Fig. 14. Loss modulus of pure polyamide 12 and studied hybrid materials at 250 °C.

Table 5
Slope of the loss modulus in the terminal region for the Pglass/LDPE hybrids

Volume percent Pglass	Slope of G'' at 190 °C	Slope of G'' at 250 °C
0	0.99	1.00
1	0.99	0.97
2	1.00	0.97
5	0.99	0.89
10	1.00	0.68

development, and temperature dependence (or independence) of polymer blends [2,63,81,90,91]. The temperature independence of a Han plot is a necessary condition for time–temperature superposition to apply to a material. However, materials that display temperature-independent Han plots do not necessarily have to superimpose. Fig. 15 displays the Han plots for pure polyamide 12 and the hybrids over a range of temperatures. Temperature independence is observed for the pure polyamide 12 and the hybrid containing 1 vol% Pglass (Fig. 15b) like others have reported for immiscible blends [81,90,91]. A small amount of scatter is evident in Fig. 15b at low moduli values and is attributed to limitations of the rheometer used. The observed temperature independence behavior for the 1 vol% hybrid indicates good compatibility between the hybrid phases and a microstructure that is unaffected by temperature. As the volume percent of Pglass is increased in the system, the temperature independence of the Han plots breaks down. Upon

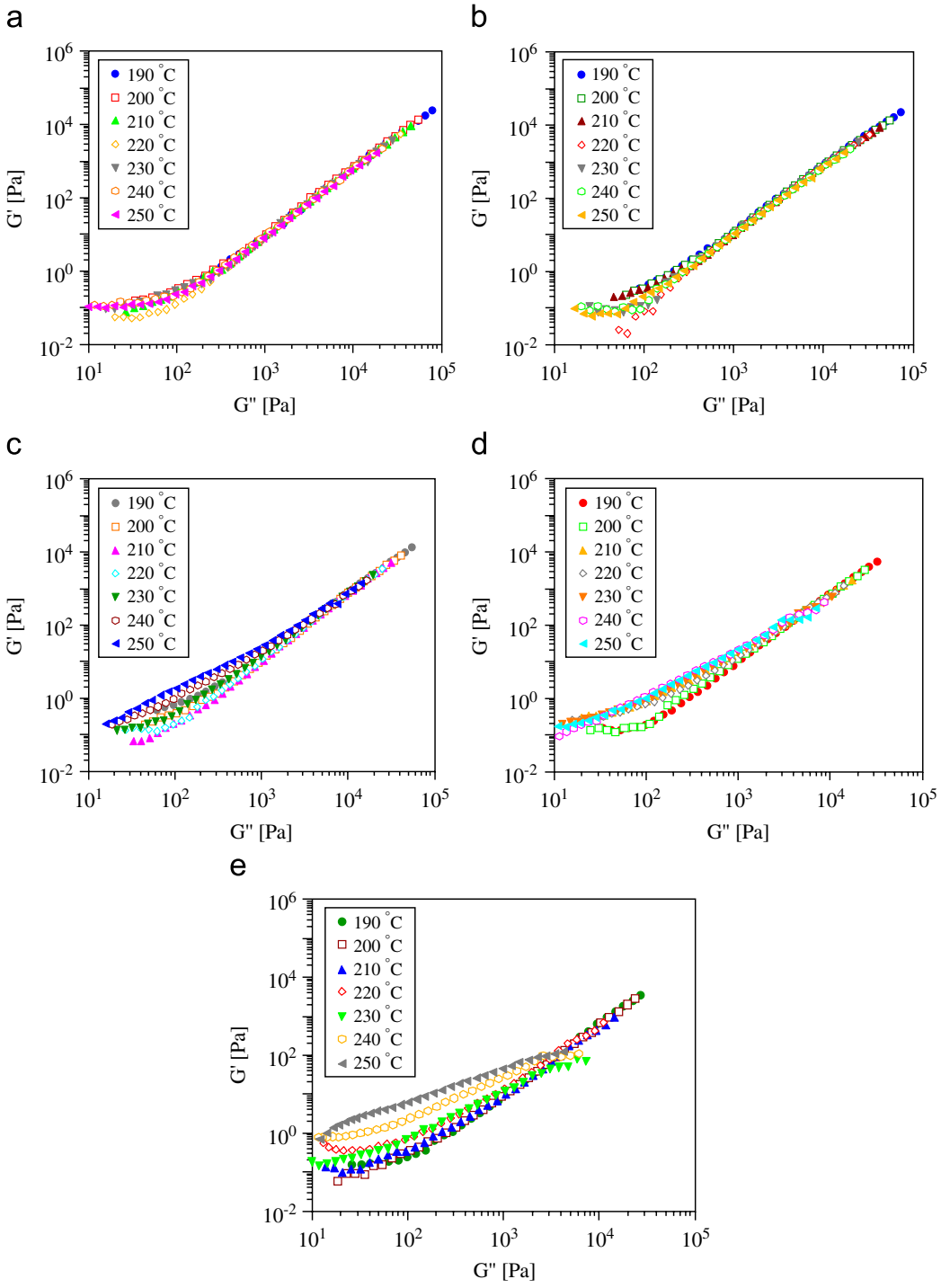

Fig. 15. Storage modulus versus loss modulus at various temperatures for (a) pure polyamide 12 and hybrids containing 1 (b), 2 (c), 5 (d), and (e) 10 vol.% Pglass.

closer examination, it can be seen that the break down occurs at 220 °C and the deviation from temperature independence increases with increasing Pglass content. Some microstructural change must be occurring at this temperature, resulting in a change in the rheological behavior of hybrids containing >2 vol% Pglass.

Researchers have also found it useful to compare different compositions of a blend at a single temperature using a Han plot [2,90]. Fig. 16 shows the Han plots of the pure polyamide 12 and the hybrids at 190, 220, and 250 °C. At 190 °C, all of the hybrids show Han plots that are independent of composition, indicating a similar morphological

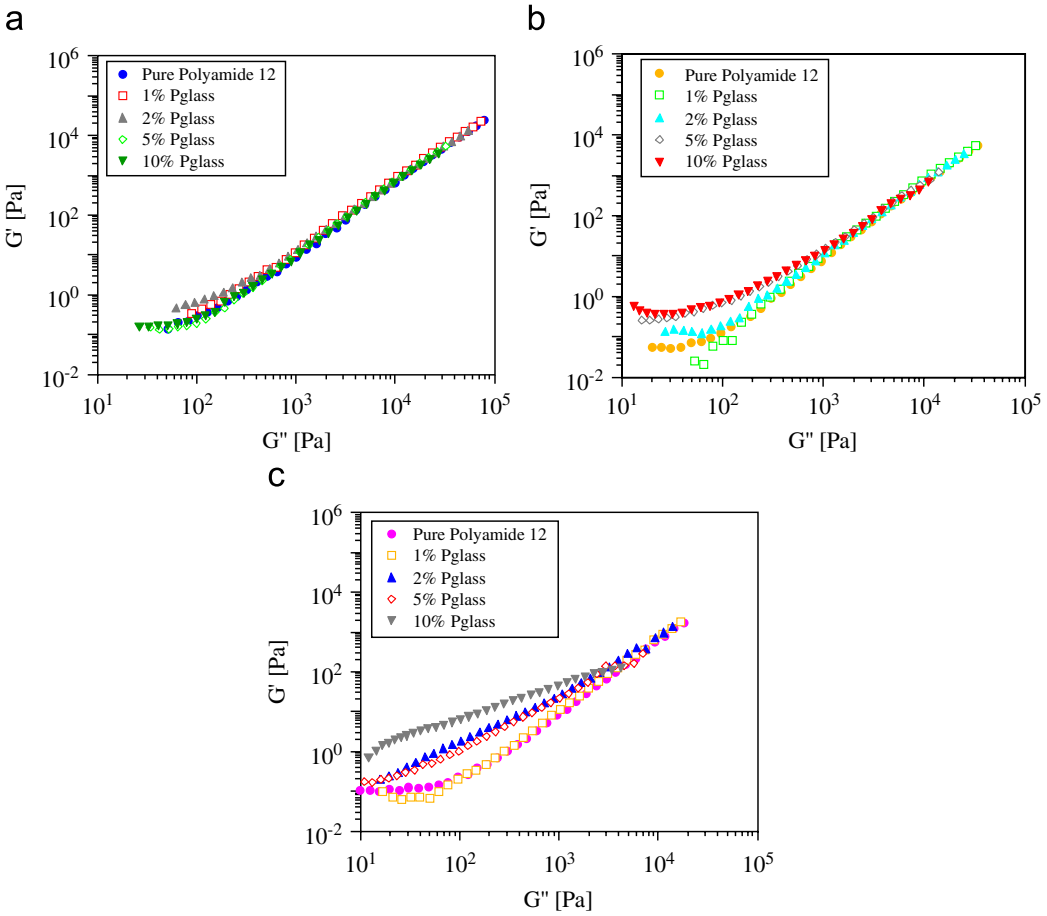

Fig. 16. Storage modulus versus loss modulus for pure polyamide 12 and studied hybrids at (a) 190 °C, (b) 220 °C, and (c) 250 °C.

state and good compatibility between the phases [90]. When the temperature is increased to 220 °C, compositional independence of the Han plots over the studied range no longer exists except for the hybrids containing $\leqslant$2 vol% Pglass which shows some evidence of compositional independence as Fig. 16b illustrates. When the temperature is further increased to 250 °C, compositional independence of the Han plots is completely eliminated. This observed change in the compositional independence behavior is believed to be due to a morphological evolution caused by the increasing temperature. We conjecture that elevated temperatures increase the miscibility of the phases, leading to a partially miscible material in the liquid (melt) state and a change in the overall morphology of the material.

Fig. 17 displays SEM micrographs of the hybrids taken before rheological measurements were performed. The figure shows that Pglass is dispersed as small droplets within the polyamide 12 matrix and the average diameter of the particles is given in Table 6. Using the droplet size calculated from Fig. 17, the applicability of the Palierne emulsion model to this system can be determined and an interfacial tension estimated [49,50]. The Palierne emulsion model has been used extensively in the literature by researchers on many different systems to estimate either the size of a dispersed phase or the interfacial tension between components [49,92–94]. The Palierne model equation (5) expresses the complex modulus of an emulsion where the dispersed phase is spherical in terms of the phases, interfacial tension, volume fraction, and radius of the dispersed phase according to the following equation:

$$G^* = G_c^* \left(\frac{1 + 3\phi H}{1 - 2\phi H} \right). \tag{5}$$

In Eq. (5), G^* is the complex modulus of the emulsion, G_c^* is the complex modulus of the continuous phase, ϕ is the volume fraction of the dispersed phase, and H is defined as follows:

$$H = \frac{(G_d^* - G_c^*)(19G_d^* + 16G_c^*) + (4\Gamma_{12}/r_d)(2G_d^* + 5G_c^*)}{(2G_d^* + 3G_c^*)(19G_d^* + 16G_c^*) + (40\Gamma_{12}/r_d)(G_d^* + G_c^*)}. \tag{6}$$

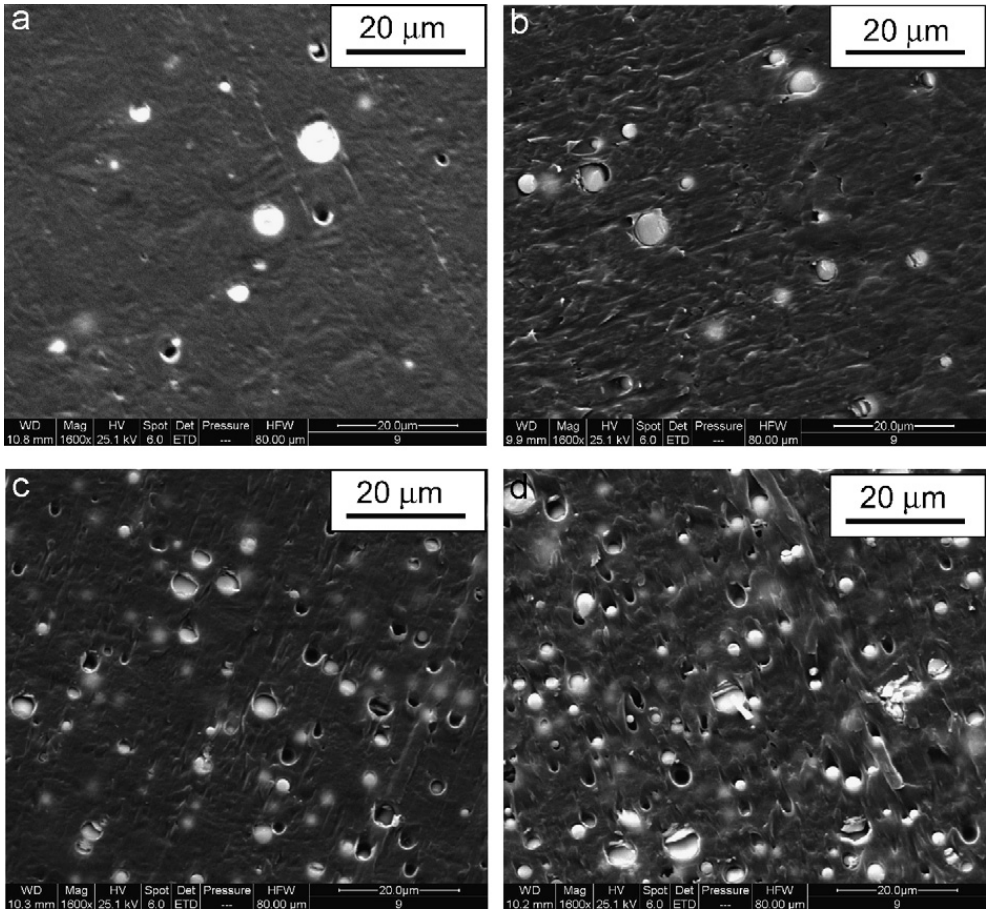

Fig. 17. Micrographs of (a) 1 vol.% Pglass, (b) 2 vol.% Pglass, (c) 5 vol.% Pglass, and (d) 10 vol.% Pglass/polyamide 12 hybrids.

Table 6
Average size of Pglass droplets in the polyamide 12 matrix

Volume percent Pglass	Average diameter (μm)
1	5.06±2.553
2	3.18±1.303
5	2.09±0.658
10	1.69±0.236

In Eq. (6), G_d^* is the complex modulus of the dispersed phase, r_d is the radius of the dispersed droplets, and Γ_{12} is the interfacial tension between the phases. From the small amplitude oscillatory shear tests that were performed on the current hybrid samples and from the micrographs, all of the variables in Eqs. (5) and (6) are experimentally determined except for the interfacial tension. Therefore, if the model provides a good fit to the data, an estimation of the interfacial tension can be made. Fig. 18 shows attempts to fit the Palierne model to the storage modulus of the hybrid containing 10 vol% Pglass at 190 and 250 °C. The model does not provide an adequate fit of the data at 190 °C. This is most likely due to the strong negative deviations from the log-additivity rule at this

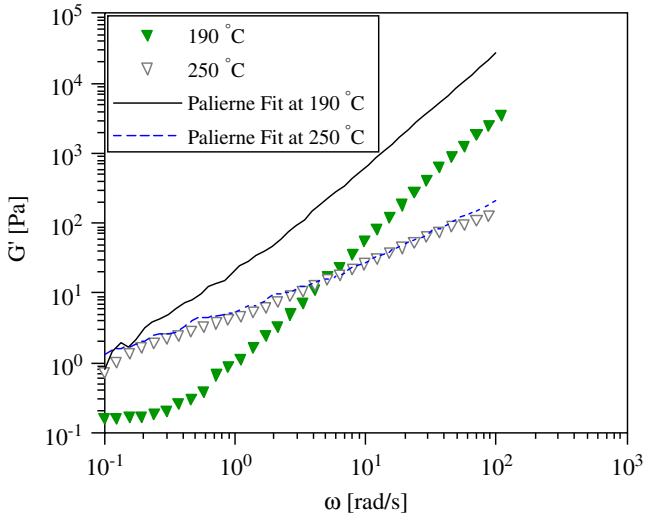

Fig. 18. Fit of the Palierne model to the storage modulus of the polyamide 12 hybrid containing 10 vol.% Pglass at the temperatures indicated.

temperature as already discussed. Since the hybrids display a much lower complex viscosity than either of the pure components, the model is unable to successfully predict the viscoelastic behavior of the hybrid. However, the model accurately predicts the storage modulus behavior at 250 °C using a value of 0.002 for the quantity of Γ_{12}/r_d. Using the average radius of a Pglass droplet found in the 10 vol% hybrid, an interfacial tension of 1.69 nN m is calculated. This extraordinarily small interfacial tension indicates the very favorable interaction that take place in this material at elevated temperatures. It also gives further support to the argument that the polyamide 12 and the Pglass phases display partial or complete miscibility at elevated temperatures.

4.3. Pglass/polyamide 6 hybrids

The strong interaction between the Pglass and the polyamide 12 matrix yielded a hybrid with unique flow properties that have not been previously observed for any Pglass/polymer hybrid. By changing the polymer matrix to polyamide 6 from polyamide 12, the sites for potential interaction between the Pglass and the polymer are effectively doubled. The strength of the interactions (i.e., degree of miscibility) between the two components of a hybrid or classical polymer blend will greatly affect the final properties of the material. While the effect of interactions and miscibility on morphology has been studied for many different classical polymer blends [95–97], there are relatively few investigations on the miscibility of polyamides with other polymers, and no reported studies on the interactions with an inorganic component [98,99]. Using melting point depression techniques, the miscibility and the chi (χ) interaction parameter for a polyamide 6 and Pglass hybrid were investigated and the resultant properties reported [40].

Melting point depression is a very good indication of miscibility between two polymers. The drop in melting point is attributed to thermodynamically favorable interactions between the polymers. The melting point depression has been used in the literature to successfully calculate χ between two components of a polymer blend in a number of different systems [98,100–102]. One such treatment of melting point depression was reported by Nishi and Wang [103]. Nishi and Wang based their work on that previously reported by Flory and Huggins, who described the interaction between polymers under thermodynamic equilibrium, as follows [104]:

$$\frac{1}{T^0_{mb}} - \frac{1}{T^0_m} = -\frac{RV_c}{\Delta H^0_f V_a} \times \left[\frac{\ln \phi_c}{x_c} + \left(\frac{1}{x_c} - \frac{1}{x_a}\right)(1-\phi_c) + \chi(1-\phi_c)^2\right]. \quad (7)$$

In this equation, $T_m{}^0$ and $T_{mb}{}^0$ are the equilibrium melting points of the crystalline polymer and the blend or hybrid, respectively. The subscripts a and c refer to the amorphous and crystalline components of the hybrid, V is the molar volume of the repeat unit of the polymer, ϕ is the volume fraction of the specified component, and R is the universal gas constant. ΔH^0_f is the heat of fusion of the crystalline component, x is the degree of polymerization and χ is the Flory–Huggins χ interaction parameter. For a large degree of polymerization that is typical of polymers, and neglecting the entropic contributions, Nishi and Wang showed that Eq. (7) reduces to Eq. (8). It should be noted, that Eq. (8) suggests that melting point depression must be due to some level of miscibility between the components of the material system.

$$\frac{1}{T^0_{mb}} - \frac{1}{T^0_m} = \frac{-RV_c}{\Delta H^0_f V_a}\chi\phi_a^2. \quad (8)$$

Plotting the left-hand side of Eq. (8) versus the volume fraction of the amorphous component squared should result in a straight line that passes through the origin. From the slope of this line, Nishi and Wang were able to determine χ for a polymer blend of an amorphous and a semi-crystalline polymer.

In the case of the Pglass/polyamide 6 hybrids, the Pglass was taken as the amorphous polymer [40]. Phosphate glasses are well known to be completely amorphous and have distributions of chain lengths and are considered to be inorganic polymers [20,22,34–36]. The heat of fusion value of the polyamide 6 used in the present calculations was 190 kJ/kg [105]. It is also necessary to determine the equilibrium melting points of the pure polyamide 6 and the hybrids. The equilibrium melting points were determined using the Hoffman–Weeks approach [106]. In this method, the equilibrium melting point is derived by plotting the observed melting point (T_m) versus the crystallization temperature (T_c). This should result in a linear plot [106]. The intersection of this plot with the line $T_c = T_m$ is taken to be the equilibrium melting point of the material. Although the Hoffman–Weeks approach does not account for lamellar thickening,

it is widely used to determine the equilibrium melting temperatures for many polymer systems [107]. Fig. 19 illustrates typical Hoffman–Weeks plots that were obtained for the hybrid materials. For the purpose of clarity, the observed equilibrium melting points for the Pglass/polyamide 6 hybrids are reported in Table 7. The equilibrium melting point value for the pure polyamide 6 agrees with values reported in the literature [108]. By plotting the melting point depression as a function of the volume fraction of Pglass, a straight line with an intercept close to zero is obtained (Fig. 20). The fit of the linear line gives an R^2 value greater than 0.98. Using the slope of the line from Fig. 20, and Eq. (8), χ was calculated to be −0.067. This value satisfies the condition for polymer miscibility and indicates that the Pglass and the polyamide 6 are indeed miscible in the melt. To our knowledge, this is the first reported evidence of miscibility of inorganic glass and organic polymer, and is considered to be an important finding that may stimulate future research studies, leading to a better understanding of the structure and properties of these remarkable hybrid inorganic and organic polymeric materials.

Both the dynamic and tensile mechanical properties of this new hybrid material were also studied. A graph of the loss modulus versus temperature data is shown in Fig. 21. It is clearly evident from this figure that as Pglass is added to the polyamide 6 matrix, the T_g of the polyamide 6 decreases. Additionally, no glass transition peak is observed for the pure Pglass component in the hybrid, which should appear around 125 °C. Attempts to model

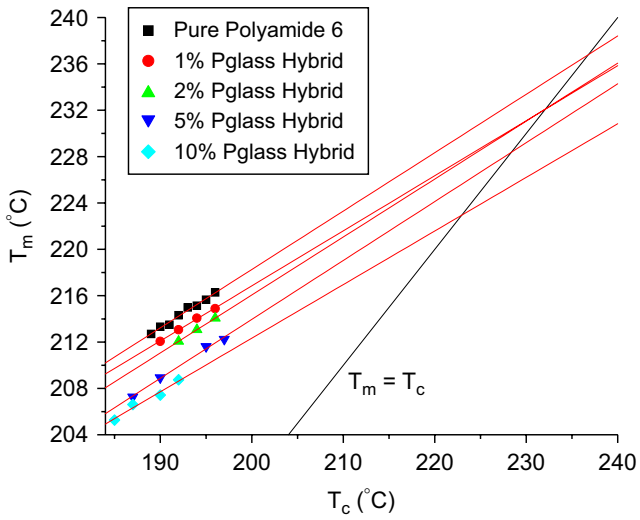

Fig. 19. Hoffman–Weeks plots for the Pglass/polyamide 6 hybrid materials with the Pglass volume percent indicated.

Table 7
Equilibrium melting points (T_m^0) of pure polyamide 6 and its hybrids determined from DSC measurements

Volume percent polyamide 6	Volume percent Pglass	T_m^0 (C)
100	0	236
99	1	232
98	2	232
95	5	228
90	10	222

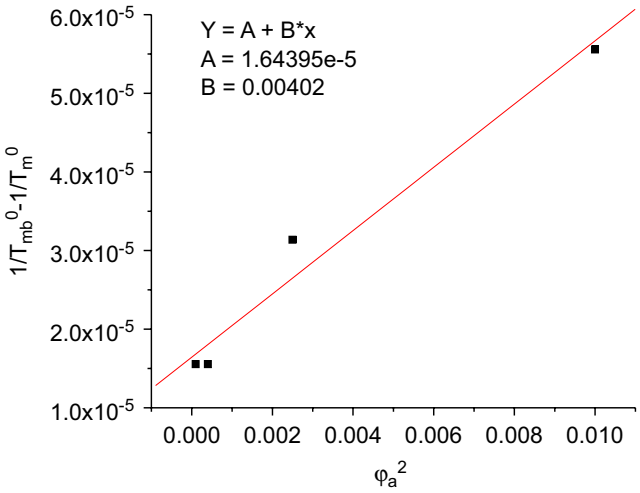

Fig. 20. Melting point depression of the Pglass/polyamide 6 hybrid as a function of composition.

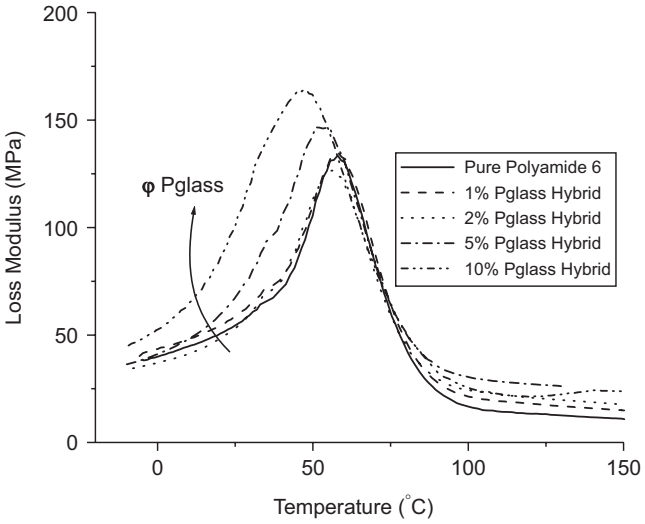

Fig. 21. Loss modulus versus temperature from torsional dynamic mechanical analysis for the Pglass/polyamide 6 hybrid materials with the Pglass volume percent indicated. The arrow shows the direction of increasing volume percent of Pglass (φ Pglass).

the glass transition temperature of the hybrids with empirical equations in the literature such as the Fox [109] or the Gordon-Taylor [110] equations failed because these equations predict a glass transition value that is between the glass transition temperatures of the individual components. From these results, it appears that the Pglass is acting as a macromolecular plasticizer for the polyamide 6. It is worthy to note that phosphates are used as plasticizers for various polymers; however, they (phosphates) are typically small molecules, unlike the Pglass used in this study [111]. It is important to note that there are other previously reported cases of organic macromolecular plasticizers [100,111], but no prior reported case of inorganic Pglasses as described in this article.

The tensile mechanical properties of the hybrids are shown in Fig. 22, which depicts typical stress/strain curves for these hybrid materials. Clearly, this figure shows that the addition of Pglass affects the failure mechanism of the hybrid in an intriguing manner as shown by the varying shapes of the curves with varying Pglass volume content. The yield point becomes more obvious as more Pglass is added ($\geqslant 5$ vol%) to the polyamide 6. The stress/strain curves for the pure polyamide 6 and the hybrids with Pglass volume percent ($\leqslant 2\%$) are typical of viscoelastic materials, being concave to the strain axis and showing no clear evidence of a yield stress. At higher Pglass volume percents ($\geqslant 5\%$), the curves are consistent with that of a pseudo-ductile material showing a clear evidence of a yield stress, followed by a monotonic increase in stress with increasing strain as the material approaches failure. This behavior is akin to that of typical plasticized polymers reported in the literature [112].

As can be seen from Table 8, the Young's Modulus of the hybrid material is significantly less than that of the pure polyamide 6. The addition of the Pglass causes the polyamide to be less stiff. This behavior is also reflected in the strain at break values for the hybrid materials. The hybrids typically break at larger strains than that of the pure polyamide. It is reasonable to expect this trend to begin to reverse at some composition much greater than 10% Pglass where the increase in elongation would be offset by the brittle nature of the Pglass component, thereby causing failure at a relatively low strain. Work is in progress in the author's laboratory to confirm this hypothesis. Table 8 also displays the energy to break as a function of composition. Energy to break is related to the area underneath a stress–strain curve. Although energy to break is dimensionally dependent, it gives a qualitative indication of the toughness of the material. While the addition of up to 5% by volume of Pglass generally preserves the toughness of the pure polymer material, the 10% Pglass composition does show a marked

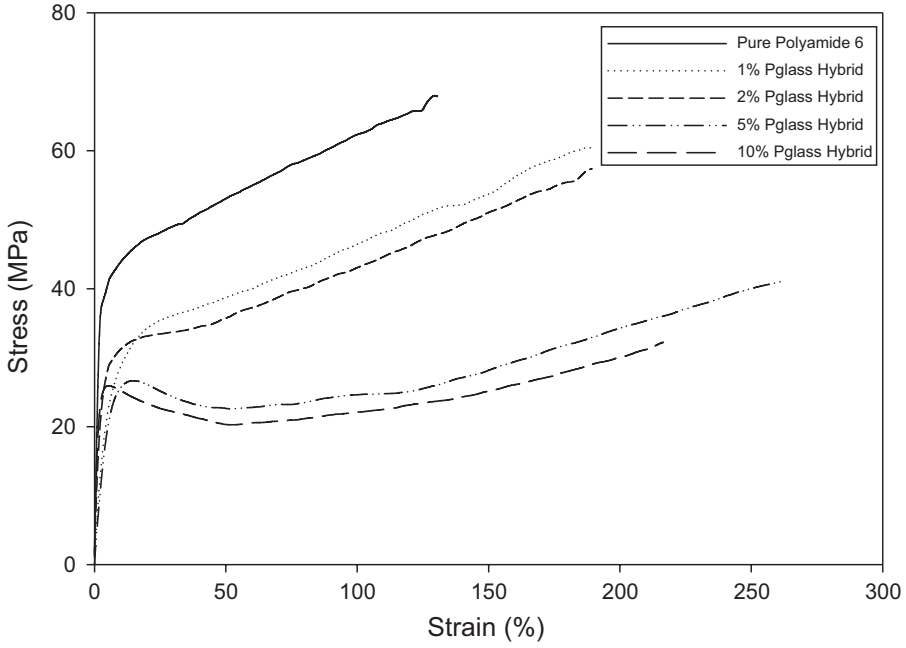

Fig. 22. Typical stress/strain curves for Pglass/polyamide 6 hybrid materials with the Pglass volume percent indicated.

Table 8
Summary of properties from tensile mechanical testing of the Pglass/polyamide 6 hybrids

Volume percent polyamide 6 in hybrid	Young's modulus (MPa)	Strain at break (%)	Energy to break (MJ/m^3)
100	1053 ± 52	177 ± 33	102 ± 20
99	539 ± 25	211 ± 19	103 ± 12
98	523 ± 19	190 ± 12	83 ± 5
95	472 ± 23	288 ± 46	81 ± 24
90	558 ± 36	249 ± 17	62.1 ± 6

decrease. This is most likely due to the brittle nature of the Pglass component.

The mechanical properties of the hybrid materials are both interesting and *counterintuitive*. Typically, as conventional solid glass filler is added to a polymer system, an increase in Young's modulus and a decrease in the strain at break is observed [112]. However, the observed mechanical properties of the hybrids are remarkably similar to that obtained when a plasticizer is added to a pure polymer [113,114]. This is further evidence indicating that the Pglass is acting as a macromolecular plasticizer for the pure polyamide 6.

While it has been established that polyamide 6 and Pglass form a single phase in the liquid state, the origin of the solid-state properties and the plasticization behavior cannot be explained by melt miscibility. This is a matter for further studies. Note however that similar reductions of the T_g have been observed for several nanocomposite systems [115–117]. Ash et al. [115,116] found that the addition of <1 wt% of spherical alumina nanoparticles to poly(methyl methacrylate) caused a T_g reduction of 25 °C[111,156]. This behavior was conjectured to be the result of the formation of an interaction zone, which is a highly mobile liquid-like area. This region of mobility disrupts the percolation of the slower moving regions and results in a decrease of the T_g [116]. Similar T_g reductions were observed for polymers containing polyhedral oligomeric silsesquioxane (POSS). While the observation of accelerated glass transition relaxations in Pglass/polyamide 6 hybrids was studied via dynamic mechanical analysis (DMA), it is also possible to use broadband dielectric relaxation spectroscopy to study the relaxation behavior of these materials.

Two areas of polymer science and technology that have greatly benefited from the use of DRS are miscible polymer blends and polymer composites. Several researchers have used DRS to examine the degree of miscibility in polymer blends and peak shifts and peak broadening that are commonly observed for miscible or partially miscible polymer blends [118–122]. However, strong interaction between two organic polymers is not the only factor that can influence the relaxation behavior of polymers. The addition of inorganic fillers to a polymer matrix also greatly influences the relaxations of the polymer. It has been shown by Perrin et al. [123] that the formation of a nanoscale inorganic sol–gel network causes a broadening of the isochronal dielectric loss curve as well as regions of restricted polymer mobility. Traditional clay/polymer nanocomposites have also been studied via DRS [124,125]. Lee et al. [125] found that exfoliated clay/polyamide 11 nanocomposites greatly accelerated the T_g (α−relaxation) of the polymeric component. It was suggested that the clay greatly diminished intermolecular cooperativity, which resulted in an accelerated α relaxation.

Fig. 23 is an isochronal graph of the temperature dependence of dielectric loss of the pure hybrid components and of a typical Pglass/polyamide 6 hybrid containing 10 vol.% Pglass. Three relaxations can be identified in both the hybrid and the pure polyamide 6. These relaxations have been previously reported for pure polyamide 6 [126–129]. The low temperature γ-relaxation involves the motion of very short $-CH_2$ segments and an amide group which provides the dielectric activity. Assignment of the molecular motions associated with the

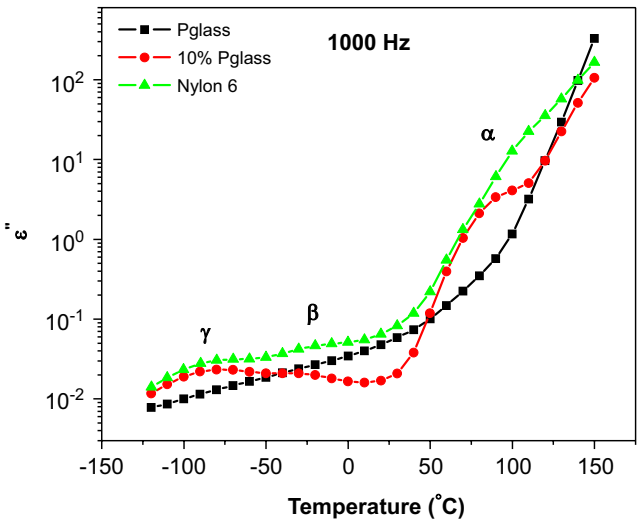

Fig. 23. Temperature dependence of the dielectric loss for the pure components and the 10 vol.% Pglass/polyamide 6 hybrid.

mid-temperature range relaxation (i.e., β-relaxation) is more complicated and a number of opinions on their molecular origins are reported in the literature. For example, Frank et al. attributes the β-relaxation to the movement of more extended $-CH_2$ segments as well as motions of the amide groups [126]. These motions are exacerbated by the presence of water in the system. Laredo et al [127] reported that the β-relaxation is due solely to firmly bound water that is often present in polyamides despite drying that can be completely eliminated only by extremely rigorous drying procedures. In the research monograph by McCrum and Williams [129], the dielectric β-relaxation was attributed to $-NH_2$ and –OH chain end group movements by some research groups, while other researchers attributed it to the motion of a water–polymer complex. In the current work reviewed here, the effect of water on the β-relaxation is considered to be negligible due to the initial drying procedure that was performed on the materials prior to testing. If any small amount of water remained in the materials, it was firmly bound water. Additionally, similar amounts of bound water should be present in all tested samples, thereby making direct comparison of results possible. The α-relaxation (the highest temperature relaxation) is connected with the onset of large-scale motions of the chain segments in the vicinity of the T_g. The pure Pglass only displays a single relaxation, which is not seen in the isochronal graph due to the high conductivity of the pure Pglass at elevated temperatures. The 10 vol% Pglass/polyamide 6 hybrid also displays an increase in permittivity at elevated temperatures, but this should not be confused with its α-relaxation process, which is clearly evidenced by the peak at approximately 75 °C. However, this α-relaxation process can be clearly seen in isothermal graphs, as will be discussed later. This relaxation in the pure Pglass, which we label as the α-relaxation, is similar to the dipole losses observed for polymers, but is most likely due to separated ion pairs [130]. From Fig. 23, it is easily observed that the hybrid's α-relaxation occurs at a lower temperature than either of the pure components, indicating a physiochemical interaction between the hybrid components. In addition, the hybrid displays a single α-relaxation which seems to indicate that the Pglass domains are not large enough to contribute to the appearance of a fourth relaxation in the hybrid. The appearance of a single T_g is often used as a criteria for miscibility in classical polymer blend systems where the blend T_g is typically between that of the pure components [100,110,131,132].

While the appearance of a single T_g in the hybrid suggests partial miscibility, the temperature reduction of the T_g is not explained in the miscible polymer blend literature. Similarly, the β-relaxation of the hybrid appears at a reduced temperature when compared to that of the pure polyamide 6. However, the γ-relaxation remains relatively unaffected. These effects are more clearly observed in isothermal curves as shown in Fig. 24. Fig. 24a displays the dielectric loss as a function of frequency at −40 °C for the pure polyamide 6 and the 10 vol% Pglass hybrid. The pure Pglass was omitted in Fig. 24a because it shows no relaxation at this temperature. Although the γ-relaxations of the pure polyamide 6 and the hybrid are almost identical, the β-relaxation of the hybrid has shifted to a significantly higher frequency and has almost become a shoulder in the hybrid's γ-relaxation. In Fig. 24b, the dielectric loss as a function of frequency is shown for both pure components as well as the hybrid at the relatively higher temperature of 80 °C, which is in the range of the α-relaxation process. At this temperature, one can see that the polyamide 6 shows a β-relaxation process with a maximum frequency (f_{max}) of about 3×10^5 Hz. In addition, the α-relaxation process of the polyamide 6 appears with an f_{max} of around 10^2 Hz. For the Pglass, the α-relaxation appears at an f_{max} of 5 Hz. On the other hand, only one relaxation process, the α-relaxation, is observed for the hybrid at $f_{\max} \approx 7 \times 10^2$ Hz. The β-relaxation process of the hybrid has shifted to a higher frequency that is outside the range of equipment used for the measurement. Further, it is noteworthy that the observed height of the α-relaxation process in the hybrid is below that of either of the pure components.

It is possible to model these molecular relaxations using the well-known phenomenological Havriliak–Negami (HN) equation with an added ionic conductivity term as shown below [129,133–135a,b]

$$\varepsilon^*(\omega) = \varepsilon' - i\varepsilon'' = -i\left(\frac{\sigma_0}{\varepsilon_0 \omega}\right) + \sum_{k=1}^{3}\left[\frac{\Delta\varepsilon_k}{(1+(i\omega\tau_k)^{a_k})^{b_k}} + \varepsilon_{\infty k}\right]. \quad (9)$$

In this equation, ε^* is the complex dielectric constant. The energy storage per cycle and the energy loss or absorption per cycle are represented

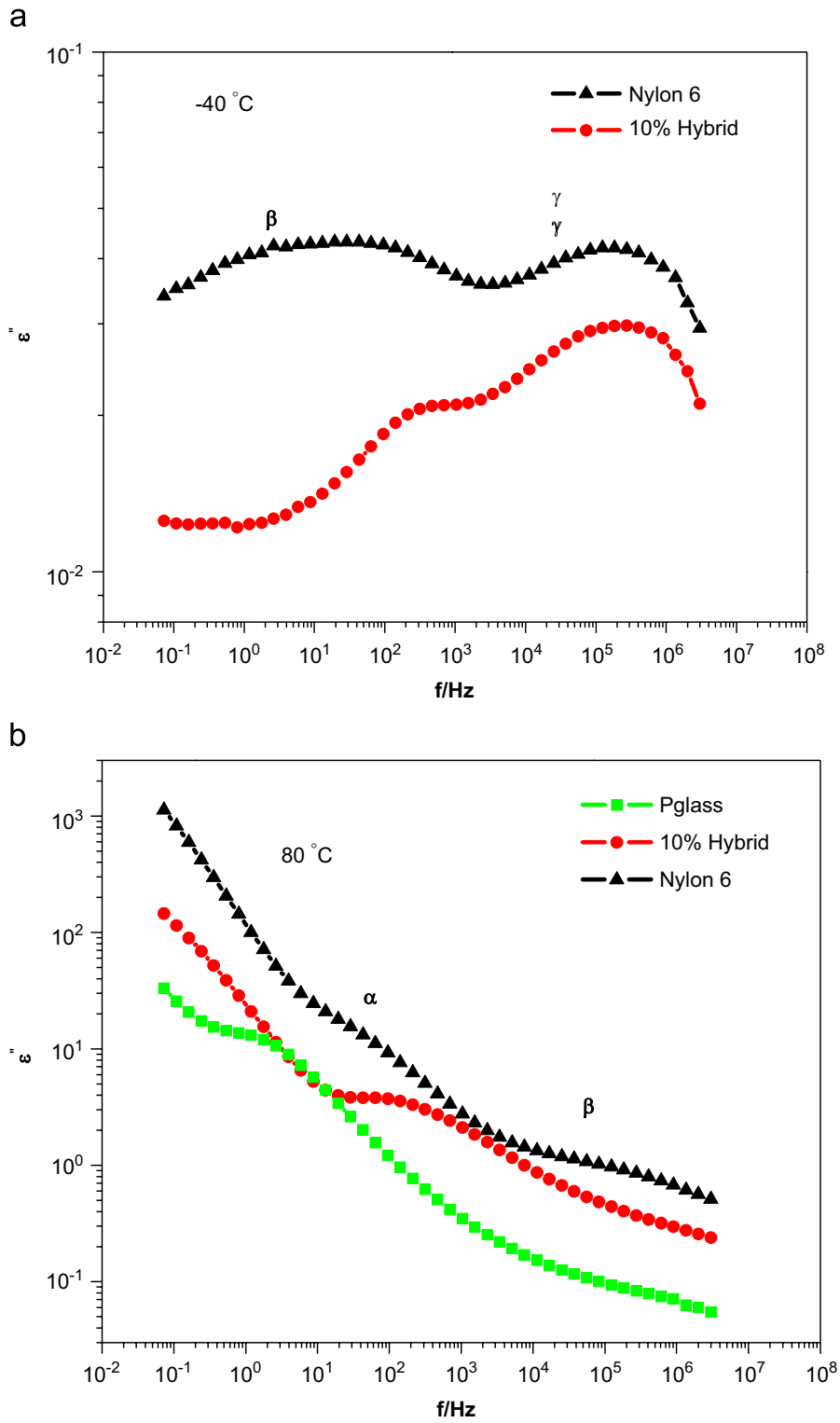

Fig. 24. Dielectric loss as a function of frequency at (a) −40 °C and (b) 80 °C for the pure components and the 10 vol.% Pglass/polyamide 6 hybrid. Note that in (a) Pglass data are omitted because it displays no relaxation at this temperature.

by ε' and ε'', respectively. σ_0 is the dc conductivity, ε_0 is the permittivity of free space (8.854 pF/m), ω is the angular frequency and i is equivalent to $-1^{1/2}$. $\Delta\varepsilon_k$ is the strength of the kth relaxation, $\varepsilon_{\infty k}$ is the high-frequency relative permittivity of the kth relaxation, and τ_k is the characteristic relaxation time of the kth component. The exponents a and b are distribution parameters that describe the

Table 9
Fit parameters of the HN equation of the α-relaxation of the pure components and the 10 vol.% Pglass/polyamide 6 hybrid at 80 °C

Volume percent Pglass	a	b	$\Delta\varepsilon$
0	0.8489	0.6162	25.58
10	1	0.3239	11.02
100	0.8506	1	15.17

symmetric and asymmetric broadening of the relaxation time distribution function, respectively. When $a = 1$, the HN equation reduces to the Davidson–Cole expression and when $b = 1$, the Cole–Cole function is obtained. In the special case of a and b both being equal to unity, the Debye equation is obtained. The fit is quite good and the characteristic relaxation time for each relaxation process can be extracted [135b]. Table 9 displays the fit parameters of the HN equation to the α-relaxation of the pure Pglass, pure polyamide 6, and the hybrid at 80 °C (data of Fig. 24b).

The temperature dependence of the characteristic relaxation times of the T_g-like relaxations (i.e., α-relaxations) can then be described using the following Volger–Fulcher–Tammann (VFT) equation [136]:

$$\tau(T) = \tau_0 \exp\left(\frac{E_a}{k_B(T - T_V)}\right). \quad (10)$$

In the VFT equation, k_B is the Boltzmann constant, E_a is apparent (temperature-dependent) activation energy, T_V is a hypothetical temperature at which segmental motions are frozen-in, and τ_0 is a hypothetical relaxation time at infinite temperature. Fig. 25 displays the characteristic relaxation time as a function of inverse temperature. The solid lines represent fits of the data to the VFT equation and Table 10 displays the fitting parameters. Obviously, the figure shows that addition of Pglass to the polyamide 6 accelerates the α-relaxation of the polymer chains. In turn, the hybrid displays lower apparent activation energy as compared to that of the pure components. It is noteworthy that reduction of a polymer blend's T_g and its apparent activation energy are often attributed to partial miscibility of the pure components in polymer blends [121,122]. A similar mechanism is considered to be operating in the current hybrid system. The Pglass seems to accelerate the motions of long chain segments of polyamide 6 in the Pglass/polyamide 6 hybrid, but it (Pglass) is unable to significantly

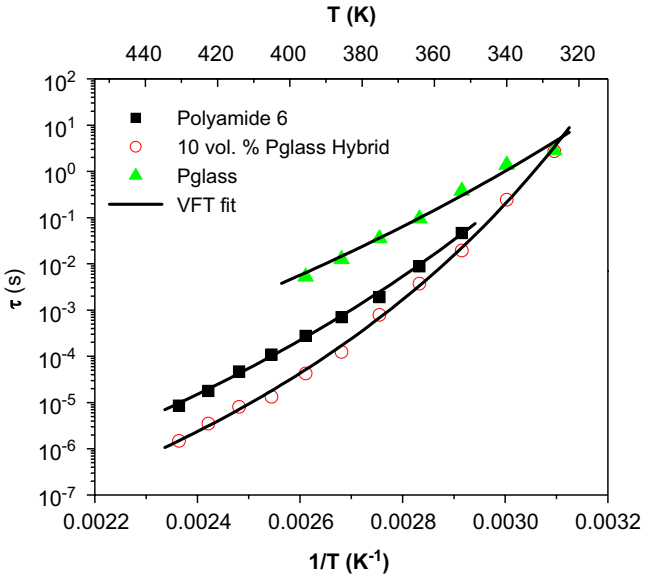

Fig. 25. The characteristic relaxation times of the α-relaxation of the pure components and 10 vol.% Pglass/polyamide 6 hybrid as a function of temperature (solid lines represent fits of the VFT equation).

Table 10
Fit parameters of the VFT equation

	Pglass	Hybrid	Polyamide 6
τ_o (s)	4.003×10^{-10}	2.201×10^{-12}	3.194×10^{-12}
E_a (eV)	0.3040	0.2218	0.2853
T_0 (K)	170.4	231.3	201.3

impact very short (i.e., approximately two $-CH_2$ units) motions.

The origin of the observed glass transition temperature behavior is believed to be due to the partial miscibility of the pure components in the solid state. While previously reported experimental evidence has shown that polyamide 6 and Pglass are miscible in the liquid (melt) state, the DRS investigations performed on these materials suggest partial miscibility in the solid state. TEM investigations of the hybrid material display a two-phase microstructure with the Pglass being distributed as droplets in the polymer matrix (Fig. 26). Size analysis of the micrograph reveals an average particle size of 530 ± 5 nm, with the smallest observed particle being 70 ± 2 nm in size. The TEM also shows the spherulites (lamella) of the crystalline structure of the polyamide 6 matrix.

Although TEM can observe nanoscale particles, new advanced NMR methods can be reliably used to estimate the size and amount of Pglass that is

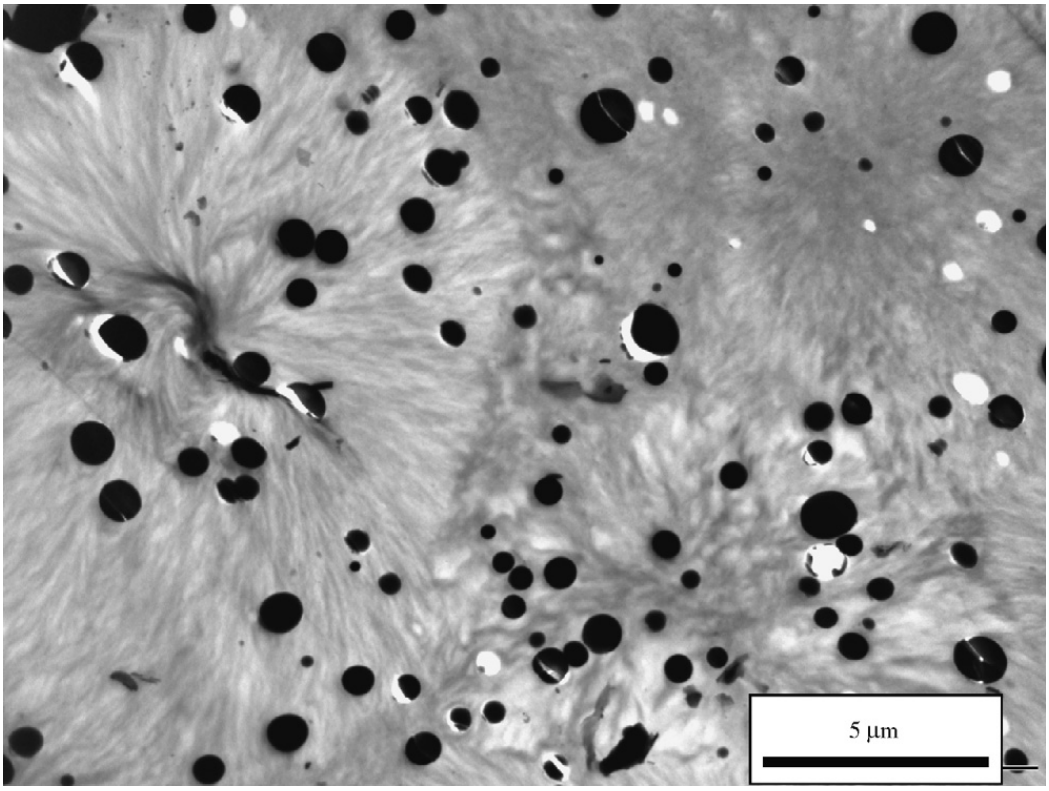

Fig. 26. TEM micrograph of the 10 vol.% Pglass/polyamide 6 hybrid.

distributed within a few nanometers (i.e. the molecular level) of polyamide 6 chains [137]. The HARDSHIP pulse sequence, which measures the dephasing of ^{31}P in the glass by matrix ^{1}H, has been successfully used to investigate the partial miscibility of the polyamide 6 and the Pglass [138a]. The HARDSHIP pulse sequence alternates REDOR (Rotational Echo DOuble Resonance) heteronuclear recoupling for ~0.15 ms with periods of homonuclear dipolar dephasing that are flanked by canceling 90° pulses. The heteronuclear evolution of the weakly coupled protons is refocused within two rotation periods. As desired, little HARDSHIP dephasing is observed in the pure Pglass, while REDOR dephasing is fast due to the ^{1}H dispersed in the Pglass. In the hybrid material, quantitative ^{1}H–^{31}P HARDSHIP after a long (50 or 200 s) recycle delay and 90°-pulse excitation (squares) shows fast initial dephasing by the polyamide protons, indicative of phosphates in intimate contact with the polyamide 6 matrix (Fig. 27). The plateau of 75% shows that the amount of Pglass within 0.7 nm from the polyamide matrix is 25% of the total. We conjecture that the partial miscibility of the Pglass in the polymer matrix affects the relaxations of the polyamide 6 chains similar to that

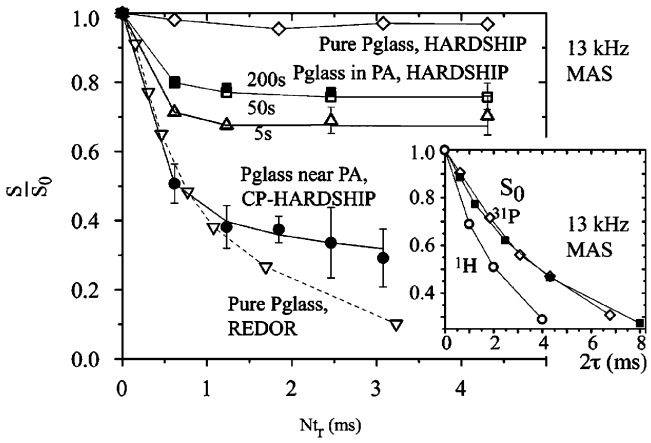

Fig. 27. ^{1}H–^{31}P HARDSHIP NMR data for determining the size and fraction of Pglass nanoparticles in the 10% Pglass/polyamide 6 (PA) hybrids. Data obtained on the pure Pglass, as well as ^{1}H–^{31}P REDOR dephasing curves, are shown for reference. Some HARDSHIP data were obtained after 90°-pulse ^{31}P excitation, with recycle delays of 5 s (open triangles), 50 s (open squares), and 200 s (filled squares, quantitative).

observed for polymers filled with nano-sized fillers. The Pglass that is distributed on the molecular level reduces the intermolecular hydrogen bonding of the polyamide 6 chains. In turn, this disrupts the network of long chains that are hydrogen bonded,

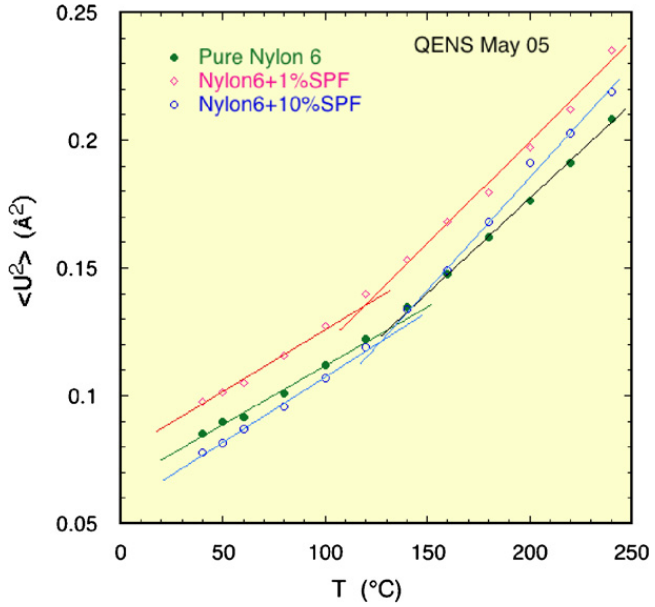

Fig. 28. The mean-square displacements of hydrogen atoms in Pglass/polymer 6 hybrids showing an enhanced mobility and differences in both $\langle U^2 \rangle$ and the slopes.

thereby creating the possibility of independent chain movement which results in an acceleration of long range segmental motions observed by both DMA and DRS techniques already discussed.

In a recent preliminary study, quasi-elastic neutron scattering (QENS) was used to probe the underlying structure and its formation for the Pglass/polyamide 6 hybrid [138b]. Fig. 28 shows the mean-square displacements of hydrogen atoms ($\langle U^2 \rangle$) as a function of temperature obtained from QENS of 0, 1 and 10% Pglass/Polyamide 6 hybrid. Enhanced average hydrogen mobility with added 1% Pglass is clearly seen from the change of the slope at a certain temperature, resulting in a more flexible dynamics. The behavior of added 10% glass is different, in both $\langle U^2 \rangle$ and the slopes, suggesting that the dynamics of the hydrogen atoms is not enhanced until above ~150 °C (Loong C.-L., Otaigbe J.U., 2005, unpublished work). There appears to be a change in the rate of increasing $\langle U^2 \rangle$ near the glass-transition point. These preliminary QENS data are very encouraging and interesting; and found to be in good qualitative agreement with the NMR and rheology data already discussed.

5. Unanswered questions and plausible solutions

The work reviewed in this article has demonstrated that new TFP glass/polymer hybrids can be developed with unprecedented properties and structures, if the interactions between the Pglass and the polymer are carefully chosen and the processing conditions are controlled. These scientifically interesting materials have a lot of promise industrially, but many fundamental science questions remain that need to be addressed before these materials can achieve their full technological potential. Some of these questions and potential approaches to addressing them are now presented in an effort to guide future experimental studies and theory development on the relatively little-studied hybrid Pglass/polymer materials.

It has been shown that the addition of Pglass to a semicrystalline polymer causes a reduction in the percent crystallinity of the polymer. This unique property of Pglass hybrids has been determined to be an experimental fact. However, the origin of the decreased crystallinity is not presently understood, and awaits further experimentation. The crystalline properties of the constituent homopolymers in a classical polymer blend have been extensively studied and reported in the literature [139–144]. One source of reduced crystallinity in classical polymer blends was ascribed to confined crystallization of polyamide 6 in a PS matrix. Polyamide 6 that was confined on the nanometer size scale had its crystallinity severely reduced [145]. While the case of reduced crystallinity due to confinement may be operating in the current Pglass/polymer hybrids at very high Pglass concentrations, it is more likely that some other mechanism may be contributing to this observed phenomenon. Light can be shed on this phenomenon using X-ray diffraction techniques. By using small angle X-ray scattering (SAXS), it will be possible to see if some fraction of the Pglass is residing inside the polymer spherulites, which would result in an increased long period of the crystallized chains. Further studies of the growth process could be carried out by applying the Lauritzen–Hoffman equation to the hybrid systems [104,142]. The Lauritzen–Hoffman equation is defined as shown below

$$\ln G + \frac{U^*}{R(T_c - T_\infty)} = \ln G_0 - \frac{K_g}{T_c(\Delta T)f}. \qquad (11)$$

where G is the crystal growth rate, G_0 is a preexponential factor, U^* is the activation energy for transporting the polymer chain segments to the crystallization site, R is the gas constant, T_∞ is a temperature below which polymer motion ceases, ΔT is the degree of supercooling, f is a correction

factor, and K_g is the nucleation constant. The variable f is defined below

$$f = \frac{2T_c}{(T_m^0 + T_c)}, \tag{12}$$

where T_c is the crystallization temperature and $T_m{}^0$ is the equilibrium melting point. The nucleation constant is also defined in terms of other variables as shown below

$$K_g = \frac{nb_0\sigma\sigma_e T_m^0}{\Delta h_f k_B}. \tag{13}$$

In this equation, n is dependent on the crystallization regime, b_0 is the molecular thickness, σ is the lateral surface free energy, σ_e is the end-surface free energy, Δh_f is the heat of fusion per unit volume, and k_B is the Boltzmann constant. Using these equations, it may be possible to determine the energy required to form a crystal structure in the presence of Pglass. This should provide further insight into the origin of the reduced crystallinity of the hybrid systems. Other X-ray diffraction studies utilizing wide angle X-ray diffraction (WAXD) techniques can be used to determine any influence of Pglass on the crystallographic structure of the polymer, i.e. inducing polymorphism in the polymer crystals [146,147].

Other areas of fundamental interest include the high degree of interaction between polyamide 6 and Pglass. While it was experimentally determined that polyamide 6 and Pglass may form a single phase in the melt, a phase diagram has still not been constructed for this hybrid. Unfortunately, this hybrid is opaque even at elevated temperatures, which precludes the use of well-established simple cloud point measurements to determine the phase diagram. However, there are alternative methods reported in the literature that may be useful. By using temperature resolved X-ray diffraction peaks, it is possible to monitor the phase change in polymer blends [148–150]. Essentially, the appearance or disappearance of an ordered phase over a range of temperatures is effectively monitored using its diffraction peak. This experimental scheme should be quite effective for the hybrid systems because the Pglass should scatter differently than the organic polymer chains.

Further understanding of the phase behavior of these hybrid materials could be generated by studying the effect of shear on both the interaction parameter and the phase diagram. It is well known that shear can have a dramatic effect on the miscibility of polymer blends [151–156]. While it may be possible to use rheology to examine this effect, it will be much more instructive to follow the phase behavior using in situ rheo-SAXS/WAXD (i.e., rheo-small angle X-ray and rheo-wide angle X-ray techniques). Rheo-SAXS and rheo-WAXD techniques have been utilized by several researchers to determine the effect of shear on crystal structure and the crystallization process of several polymers and polymer blends [157,158]. It should be possible to apply the rheo-SAXS/rheo-WAXD techniques to monitor the dissolution of the Pglass inside the polyamide 6 matrix and to determine the effect of shear upon the phase diagram of the hybrids. Rheo-SANS (i.e., rheo-small-angle neutron scattering) techniques can be used in a similar manner. Researchers have used rheo-SANS to determine the effect of shear on orientation of polymer clay solutions and on the morphology of micellar networks [159,160]. It should be possible to use small angle neutron scattering to determine the effective χ interaction parameter of a polymer blend using the equation shown below [161,162]:

$$S^{-1}(q) = \frac{1}{N_1\phi_1 S_1(q)} + \frac{1}{N_2\phi_2 S_2(q)} - 2\chi_{eff}. \tag{14}$$

In Eq. (14), $N_{1,2}$ is the number of segments in the chains of either polymer 1 or 2, $\phi_{1,2}$ is the volume fraction of component 1 or 2, $S_{1,2}(q)$ are the form factors of either component, $S^{-1}(q)$ is the structure factor of a binary blend, and χ_{eff} is the effective χ interaction parameter between the components. Combining this equation with established rheo-SANS techniques reported in the literature, it should be possible to directly calculate the effect of shear on the χ interaction parameter between the Pglass and the polyamide 6, making it possible to prepare Pglass/polymer hybrids with prescribed levels of miscibility or interaction between the pure hybrid components.

In addition to understanding the phase behavior of the Pglass/polyamide 6 hybrids, it is crucial to determine the molecular origin of this interaction. A variety of approaches will be needed to address this point. One approach might be to change the polymer matrix from polyamide 6 to another polymer of equal polarity. If melt miscibility is not observed for the new Pglass/polymer combination, then it is the amide functionality that is responsible for the high degree of interaction observed for the Pglass/polyamide 6 hybrids. It will also be instructive to change the composition of the Pglass. By

mixing the new Pglass compositions with polyamide 6 and determining the χ interaction parameter for each new hybrid, the effect of Pglass composition on miscibility will be elucidated. These techniques will provide a comprehensive understanding of the interactions between Pglass and polyamide 6.

Another important area of future research interest in this field is the generation of a wholly miscible hybrid system. Achieving a completely miscible system should generate unprecedented properties that are wholly unique to Pglass/polymer such as deformable (i.e., flexible) optical and gas/liquid barrier films hybrids. A useful starting point to determine which polymers may be miscible with Pglass is to explore polymers that are soluble in hydrochloric acid (HCl). These polymers include acrylimides, pectin, chitosan, hydroxypropyl methylcellulose, poly(2-vinyl pyridine), and poly (allyl alcohol) [105]. Because HCl can dissolve pure Pglass, there should be good compatibility with the polymers that can also dissolve in HCl. However, if this is not the case, the study may still open up the exciting possibility of preparing hybrids using a solvent casting method not presently available. Solvent-cast films will be very useful for studying equilibrium properties and generating new and unique hybrid morphologies and thin films, making the hybrids widely applicable in aggressive environments where current polymer thin films are not useable. If a miscible Pglass/polymer hybrid can be found, many pure polymer and pure glass replacement applications for the hybrids will become available or new ones with enhanced benefits may be invented. Conceptually, it may even be possible to use block copolymers, with one block being miscible with Pglass, to perform self directed assembly of nanostructured hybrids, where the Pglass is confined solely to one phase.

As already mentioned, Pglass/polymer hybrids are a unique and interesting class of materials that shows some promise of industrial importance or that is simply interesting from a scientific point of view. However, additional work remains to be done in this field to facilitate a better understanding of these hybrid materials. The aforementioned ideas suggest a few of the new and exciting directions that this field can be taken. Further, extensive investigations into the structure and properties of Pglass/polymer hybrids will allow them to fulfill their maximum technological potential, and may open up new vistas of advanced materials research. Because of their facile synthesis and desirable characteristics, the hybrid materials are expected to be excellent model systems for exploring feasibility of new routes for driving inorganic glasses and organic polymers to self-assemble into useful materials.

6. Concluding remarks and outlook

In this article, we have reviewed the current state of research into the scientifically interesting and industrially useful Pglass/polymer hybrid materials with enhanced benefits such as favorable rheological characteristics and *tunable* microstructure and properties to prescribed macromolecular structure and function. These unique materials have an incredible amount of potential and show promise to help fulfill the ever increasing demand for new, advanced materials. The hybrids described here all contain polymers that were chosen because of their commercial importance and their relative simple and well-characterized intrinsic macromolecular structure and function. These special hybrid materials belong to a class of materials that bridge the gap between conventional polymer composites and polymer blends. Because the inorganic phosphate glass is a liquid over a range of temperatures suitable for conventional polymer processing methodologies, these hybrid materials display a wide range of *tunable morphologies* that are impossible to achieve with other rigid inorganic fillers (e.g., borosilicate glass) using available methods. Additionally, the liquid nature of the Pglass at elevated temperatures allows for the fabrication of hybrids containing up to 60 vol% Pglass (i.e., ~90 wt% Pglass), thereby overcoming the intractable viscosity problem inherent to traditional polymer composites containing comparable concentrations of conventional solid fillers. Due to the wide range of size scales (i.e., from nanometer to micrometer) available to the Pglass phase of the hybrids through carefully controlled processing parameters and hybrid compositions, a large amount of surface area is available for interaction between the Pglass and the polymer phases. By controlling the interactions between the inorganic Pglass and the organic polymer phases, new materials with unprecedented properties have been achieved as already described.

We have demonstrated that Pglass/polymer hybrids with a high degree of interaction display previously unobserved properties that may make them useful for inventing a whole range of applications. The unexpected, counterintuitive results discussed in this review article are thought to be

remarkable and will provide useful guidelines to future experimental studies and theory development that explicitly takes into account the special Pglass/polymer interactions, miscibility, and microstructure evolution of the little-studied Pglass/polymer hybrid materials. Because of their facile synthesis and desirable characteristics, the current hybrid systems are expected to be excellent model systems for exploring feasibility of new routes for driving inorganic glasses and organic polymers to self-assemble into useful materials with improved properties. Conceptually, it may even be possible to use block copolymers, with one block being miscible with Pglass, to perform self-directed assembly of nanostructured hybrids, where the Pglass is confined solely to one phase. Therefore, it is likely that increased research attention will be focused in the future on these complex but important materials.

Acknowledgements

We would like to thank the US National Science Foundation Division of Materials Research (Grant Numbers NSF-DMR #97-33350 and #03-09115) and the Office of International Science and Engineering (Grant Number NSF-OISE #0436384) for funding, and K.U. thanks the Hearin Foundation for fellowship support. We thank Professor Hans Christian Öttinger's research group (especially Dr. Thomas Schweizer) at ETH, Zurich for their support during K.U.'s extended visiting graduate research assistantship at ETH. We also thank A. Rawal and Professor Klaus Schmidt-Rohr for their technical assistance with the NMR data acquisition and analysis. The technical assistance of Dr. James Kopchick and Dr. K.A. Mauritz in the acquisition of the DRS data is gratefully acknowledged. J.U.O. is indebted to his numerous collaborators at various US Government National Laboratories and in particular Drs. T. Alam (Sandia), C. Loong (Argonne), B. Sales (Oak Ridge) and M. Pruski (Ames) with whom he had the privilege to work on projects cited in this article. The research work of J.U.O's former graduate students and postdocs is gratefully acknowledged.

References

[1] Chopra D, Kontopoulos M, Vlassopoulos D, Hatzikiriakos SG. Effect of maleic anhydride content on the rheology and phase behavior of poly(styrene-co-maleic anhydride)/poly(methyl methacrylate) blends. Rheol Acta 2002;41:10–24.

[2] Nandan B, Kandpal LD, Mathur GN. Poly(ether ether ketone)/poly(aryl ether sulfone) blends: melt rheological behavior. J Polym Sci B 2004;42:1548–63.

[3] Moan M, Huitric J, Mederic M, Jarrin J. Rheological properties and reactive compatibilization of immiscible polymer blends. J Rheol 2000;44:1227–45.

[4] Paul DR, Bucknall CB, editors. Polymer blends—formulation. Polymer blends, Vol. 1. New York: Wiley; 2000.

[5] Paul DR, Bucknall CB, editors. Polymer blends—performance. Polymer blends, Vol. 2. New York: Wiley; 2000.

[6] Tucker III CL, Moldenaers P. Microstructural evolution in polymer blends. Ann Rev Fluid Mech 2002;34:177–210.

[7] Utracki LA, Kamal MR. Melt rheology of polymer blends. Polym Eng Sci 1982;22:96–114.

[8] Arkles B. Commercial applications of sol–gel-derived hybrid materials. Mater Res Bull 2001;26(5):402–8.

[9] Loy DA. Hybrid organic–inorganic materials. Mater Res Bull 2001;26(5):364–365. See also Winey KI, Vaia RA, editors. Polymer Nanocomposites. Mater Res Soc Bull 2007;32(4):314–322.

[10] Mackenzie JD. Sol–gel research-achievements since 1981 and prospects for the future. J Sol-Gel Sci Technol 2003;26:23–7.

[11] Zeigler JM, Fearon FWG, editors. Silicon-based polymer science: a comprehensive resource. Advances in Chemistry Series 224. Washington, DC: American Chemical Society; 1998.

[12] Chujo Y, Tamaki R. New preparation methods for organic–inorganic polymer hybrids. Mater Res Bull 2001;26(5):389–92.

[13] Ogoshi T, Chujo Y. Organic–inorganic polymer hybrids prepared by the sol–gel method. Compos Interfaces 2005;11:539–66.

[14] Schmidt H. Sol–gel derived nanoparticles as inorganic phases in polymer-type matrices. Macromol Symp 2000;159:434–55.

[15] Niida H, Takahashi M, Uchino T, Yoko T. Preparation and structure of organic–inorganic hybrid precursors for new type low-melting glasses. J Non-Cryst Solids 2002;306:292–9.

[16] Vaia RA, Giannelis EP. Polymer nanocomposites: status and opportunities. Mater Res Bull 2001;26(5):394–401.

[17] Krishnamoorti R, Vaia RA, editors. Polymer nanocomposites: synthesis, characterization and modeling. American Chemical Symposium Series 804. Washington, DC: American Chemical Society; 2002.

[18] Ray SS, Okamoto M. Polymer/layered silicate nanocomposites: a review from preparation to processing. Prog Polym Sci 2003;28:1539–641.

[19] Brow RK. Review: the structure of simple phosphate glasses. J. Non-Cryst Solids 2000;263–264:1–28.

[20] Otaigbe JU, Beall GH. Inorganic phosphate glasses as polymers. Trends Polym Sci 1997;5:369–79.

[21] Ray NH. Inorganic polymers. New York: Academic Press; 1978.

[22] Ray NH. The structure and properties of inorganic polymeric phosphates. Br Polym J 1979;11:163–77.

[23] Sales BC, Otaigbe JU, Beall GH, Boatner LA, Ramey JO. Structure of zinc polyphosphate glasses. J Non-Cryst Solids 1998;226:287–93.

[24] Tischendorf BC, Otaigbe JU, Wiench JW, Pruski M, Sales BC. A study of short and intermediate range order in zinc phosphate glasses. J Non-Cryst Solids 2001;282:147–58.
[25] Wiench JW Pruski M, Tischendorf BC, Otaigbe JU, Sales BC. Structural studies of zinc polyphosphate glasses by nuclear magnetic resonance. J Non-Cryst Solids 2000;263 and 264:101–10.
[26] Hoppe U, Walter G, Kranold R, Stachel D. Structural specifics of phosphate glasses probed by diffraction methods: a review. J Non-Cryst Solids 2000;263 and 264:29–47.
[27] Loong C-K, Suzuya K, Price DL, Sales BC, Boatner LA. Structure and dynamics of phosphate glasses: from ultra- to orthophosphate composition. Physica B 1998;241–243: 890–6.
[28] Crowder CE, Otaigbe JU, Barger MA, Sammler RL, Monahan BC, Quinn CJ. Melt crystallization of zinc alkali phosphate glasses. J Non-Cryst Solids 1997;210:209–23.
[29] Larson RG. The structure and rheology of complex fluids. New York: Oxford; 1999.
[30] Sammler RL, Otaigbe JU, Lapham ML, Bradley NL, Monahan BC, Quinn CJ. Melt rheology of zinc alkali phosphate glasses. J Rheol 1996;40:285–302.
[31] Sanford LM, Tick PA. Tin-phosphorous oxyfluoride glasses. 1982, US Patent: 4,314,031
[32] Tischendorf BC, Harris DJ, Otaigbe JU, Alam TM. Investigations of structure and morphology dynamics in tin fluorophosphate glass-polyethylene hybrids using solid-state ^{1}H, ^{13}C, and ^{31}P MAS NMR. Chem Mater 2002;14: 341–7.
[33] Tick PA. Tin-phosphorous oxychloride glass containing aromatic organic compounds. 1983, US Patent: 4,379,070.
[34] Tick PA. Water durable glasses with ultra low melting temperatures. Phys Chem Glasses 1984;25:149–54.
[35] Xu XJ, Day DE. Properties and structure of Sn–P–O–F glasses. Phys Chem Glasses 1990;31:183–7.
[36] Xu XJ, Day DE, Brow RK, Callahan PM. Structure of tin fluorophosphate glasses containing PbO or B_2O_3. Phys Chem Glasses 1995;36:264–71.
[37] Adalja SB, Otaigbe JU. Melt rheology of tin phosphate glasses. Appl Rheol 2001;11:10–8.
[38] Adalja SB, Otaigbe JU. Creep and recovery behavior of novel organic–inorganic polymer hybrids. Polym Compos 2002;23:171–81.
[39] Urman K, Iverson D, Otaigbe JU. A study of the effects of processing conditions on the structure and properties of phosphate glass/polyamide 12 hybrid materials. J Appl Polym Sci 2006;105:1297–308.
[40] Urman K, Otaigbe JU. Novel phosphate glass/polyamide 6 hybrids: miscibility, crystallization kinetics, and mechanical properties. J Polym Sci B 2006;44:441–50.
[41] Urman K, Schweizer T, Otaigbe JU. Uniaxial elongation flow effects and morphology development in LDPE/ phosphate glass hybrids. Rheol Acta 2007;46:989–1001.
[42] Otaigbe JU, Quinn CJ, Beall GH. Processability and properties of novel glass-polymer melt blends. Polymer Composites 1998;19:18–22.
[43] Quinn CJ, Frayer P, Beall G. Glass-polymer melt blends. In: J.C. Salamone, editor. Polymeric materials encyclopedia. New York: CRC Press; 1996. p. 2766–2777. See also Frayer PD, Monahan RJ, Pierson MD. Glass/polymer melt blends. Corning, Inc., 2001, US Patent:6268425
[44] Young RT, McLeod MA, Baird DG. Extensional processing behavior of thermoplastics reinforced with a melt processable glass. Polym Compos 2000;21:900–17.
[45] [a] Adalja SB, Otaigbe JU, Thalacker J. Glass-polymer melt hybrids. I: viscoelastic properties of novel affordable organic–inorganic polymer hybrids. Polym Eng Sci 2001;41:1055–67;
[b] Rubin II, editor. Handbook of plastic materials and technology. New York: Wiley; 1990.
[46] Guschl P, Otaigbe JU. Experimental observation and prediction of interfacial tension and viscoelastic emulsion model behavior in novel phosphate glass-polymer hybrids. J Colloid Interface Sci 2003;266:82–91.
[47] Guschl P, Otaigbe JU, Loong C-K. Investigation of phase behavior during melt processing of novel inorganic–organic polymer hybrid material. Polym Eng Sci 2004;44:1692–701.
[48] Guschl PC, Otaigbe JU. An experimental study of morphology and rheology of ternary pglass-PS-LDPE hybrids. Polym Eng Sci 2003;43:1180–96.
[49] Graebling D, Muller R, Palierne JF. Linear viscoelastic behavior of some incompatible polymer blends in the melt. Interpretation of data with a model of emulsion of viscoelastic liquids. Macromolecules 1993;26:320–9.
[50] Palierne JF. Linear rheology of viscoelastic emulsions with interfacial tension. Rheol Acta 1990;29:204–14.
[51] Carre A. Surface tension of molten glass from drop profile: application to the characterization of the interface in glass/ polymer blends. J Adhes 1995;54:167–74.
[52] Guschl PC, Otaigbe JU. The crystallization kinetics of low-density polyethylene and polypropylene melt-blended with a low-T_g tin-based phosphate glass. J Appl Polym Sci 2003;90:3445–56.
[53] Guschl PC, Otaigbe JU, Taylor EP. Engineered hybrid organic–inorganic thermoplastic materials: crystallization kinetics and tensile properties. SPE Antec Tech Papers 2003;61(2):2137–41.
[54] Young RT, McLeod MA, Baird DG. Deformation behavior of thermoplastics reinforced with melt processable glasses. SPE Antec Tech Papers 1999;57(2):2698–702.
[55] Mechbal N, Bousmina M. Uniaxial deformation and relaxation of polymer blends: relationship between flow and morphology development. Rheol Acta 2004;43:119–26.
[56] Oosterlinck F, Mours M, Laun HM, Moldenaers P. Morphology development of a polystyrene/polymethylmethyacrylate blend during start-up of uniaxial elongational flow. J Rheol 2005;49:897–918.
[57] Barnes HA. A handbook of elementary rheology. Aberystwyth: Cambrian Printers; 2000.
[58] Meissner J, Hostettler J. A new elongational rheometer for polymer melts and other highly viscoelastic liquids. Rheol Acta 1994;33:1–21 See also;
Meissner J. Development of a universal extensional rheometer for the uniaxial extension of polymer melts. J Rheol 1972;16:405–20;
Lodge AS, Meissner J. Comparison of network theory predictions with stress/time data in shear and elongation for a low-density polyethylene melt. Rheol Acta 1973;12: 41–7;
Műnstedt H. New universal extension rheometer for polymer melts 1979;23:421–36.
[59] Handge UA, Potschke P. Interplay of rheology and morphology in melt elongation and subsequent recovery

of polystyrene/poly(methylacrylate) blends. J Rheol 2004; 48:1103–22.
[60] Schulze JS, Lodge TP, Macosko CW, Hepperle J, Munstedt H, Bastian H, et al. Comparison of extensional viscosity measurements from various RME rheometers. Rheol Acta 2001;40:457–66.
[61] Guschl PC. Chemical engineering, PhD thesis. Iowa State University: Ames; 1999.
[62] Van Wazer JR. Phosphorous and its compounds, vols. I and II. New York: Wiley; 1958.
[63] Han CD, Chuang H. Criteria for rheological compatibility of polymer blends. J Appl Polym Sci 1985;30:4431–54.
[64] Utracki LA, Sammut P. Rheology of polycarbonate/linear low-density polyethylene blends. Polym Eng Sci 1990;30: 1027–40.
[65] Yoshikawa K, Molnar A, Eisenberg A. Rheological properties of blends of lithium- or sodium-sulfonated polystyrene ionomers with polyamide 6. Polym Eng Sci 1994;34:1056–64.
[66] Takahashi T, Takimoto J-I, Koyama K. Uniaxial elongational viscosity of various molten polymer composites. Polym Compos 1999;20:357–66.
[67] Chan Y, White JL, Oyanagi Y. A fundamental study of the rheological properties of glass-fiber-reinforced polyethylene and polystyrene melts. J Rheol 1978;22:507–24.
[68] Goddard JD. Tensile behavior of power-law fluids containing oriented slender fibers. J Rheol 1978;22:615–22.
[69] Hong JS, Ahn KH, Lee SJ. Strain hardening behavior of polymer blends with fibril morphology. Rheol Acta 2005;45:202–8.
[70] Valenza A, La Mantia FP, Acierno D. The rheological behavior of hdpe/ldpe blends. V. Isothermal elongation and constant stretching rate. J Rheol 1986;30:1085–92.
[71] Wagner MH, Kheirandish S, Yamaguchi M. Quantitative analysis of melt elongational behavior of LLDPE/LDPE blends. Rheol Acta 2004;44:198–218.
[72] Heindl M, Sommer M-K, Műnstedt H. Morphology development in polystyrene/polyethylene blends during uniaxial elongational flow. Rheol Acta 2004;44:55–70.
[73] Diez FJ, Alvarino C, Lopez J, Ramirez C, Abad MJ, Cano J, et al. Influence of the Stretching in the crystallinity of biaxially oriented polypropylene (BOPP) films. J Therm Anal Calorim 2005;81:21–5.
[74] Hakme C, Stevenson I, Boiteux G, Seytre G, Schoenhals A. Uniaxially stretched poly(ethylene naphthalene-2,6-dicarboxylate) films studied by broadband dielectric spectroscopy. J Non-Cryst Solids 2005;35:33–6.
[75] Marco Y, Chevalier L, Regnier G, Poitou A. Induced crystallization and orientation of poly(ethylene terephthalate) during uniaxial and biaxial elongation. Macromol Symp 2002;185:15–34.
[76] Somani RH, Yang L, Hsiao BS, Sun T, Pogodina NV, Lustiger A. Shear-induced molecular orientation and crystallization in isotactic polypropylene: effects of the deformation rate and strain. Macromolecules 2005;38: 1244–55.
[77] [a] Hersh LS, Onyiriuka EC, Hertl W. Amine-reactive surface chemistry of zinc phosphate glasses. J Mater Res 1995;10:2120–7
[b] Urman K, Schweizer T, Otaigbe JU. Rheology of tin fluorophosphate glass/polyamide 12 hybrids in the low concentration regime. J Rheol 2007, accepted.
[78] Mackay ME, Dao TT, Tuteja A, Ho DL, Van Horn B, Kim H-C. Nanoscale effects leading to non-Einstein-like decrease in viscosity. Nat Mater 2003;2:762–6.
[79] Tuteja A, Mackay ME, Hawker CJ, Van Horn B. Effect of ideal, organic nanoparticles on the flow properties of linear polymers: non-Einstein-like behavior. Macromolecules 2005;38:8000–11.
[80] Gramespacher H, Meissner J. Interfacial tension between polymer melts measured by shear oscillations of their blends. J Rheol 1992;36:1127–41.
[81] Jafari SH, Potshke P, Stephan M, Warth H, Alberts H. Multicomponent blends based on polyamide 6 and styrenic polymers: morphology and melt rheology. Polym Bull 2002;43:6985–92.
[82] Doraiswamy D, Mujumdar AN, Tsao I, Beris AN, Danforth SC, Metzner AB. The Cox–Merz rule extended: a rheological model for concentrated suspensions and other materials with a yield stress. J Rheol 1991;35(4):647–85.
[83] Feldstein MM, Kulichikhin VG, Kotomin SV, Borodulina TA, Novikov MB, Roos A, et al. Rheology of poly(*N*-vinyl pyrrolidone)-poly(ethylene glycol) adhesive blends under shear flow. J Appl Polym Sci 2006;100:522–37.
[84] Pavlinek V, Saha P. Rheological behavior of poly(methyl methacrylate) dispersions stabilized by a diblock copolymer: an anomalous viscosity-particle concentration dependence. J Rheol 1999;43:1547–54.
[85] Aubry T, Razafinimaro T, Mederic P. Rheological investigation of the melt state elastic and yield properties of a polyamide-12 layered silicate nanocomposite. J Rheol 2005;49:425–40.
[86] Osman MA, Atallah A. High-density polyethylene micro- and nanocomposites: effect of particle shape, size and surface treatment on polymer crystallinity and gas permeability. Macromol Rapid Commun 2004;25:1540–4.
[87] Park H-S, Kyu T. Rheological and mechanical characteristics of poly-*p*-phenylene terephthalamide/nylon molecular and particulate composites. Polym Compos 1989;10: 429–38.
[88] Hoffmann B, Kressler J, Stoppelmann G, Friedrich C, Kim G-M. Rheology of nanocomposites based on layered silicates and polyamide 12. Colloid Polym Sci 2000;278:629–36.
[89] Eckstein A, Friedrich C, Lobbrecht A, Spitz R, Muelhaupt R. Comparison of the viscoelastic properties of syndio- and isotactic polypropylenes. Acta Polym 1997;48(1/2): 41–6.
[90] Khonakdar HA, Jafari SH, Yavari A, Asadinezhad A, Wagenknecht U. Rheology, morphology, and estimation of interfacial tension of LDPE/EVA and HDPE/EVA blends. Polym Bull 2005;54:75–84.
[91] Zarraga A, Pena JJ, Munoz ME, Santamaria A. Thermorheological analysis of PVC blends. J Polym Sci B 2000;38:469–77.
[92] Choi G-Y, Kim H-G, Kim Y-H, Seo C-W, Choi J-H, Han D-H, et al. The rheological behavior of immiscible polymer-blends. J Appl Polym Sci 2002;86:917–24.
[93] Fang Y, Carreau PJ, Lafleur PG. Thermal and rheological properties of mLLDPE/LDPE blends. Polym Eng Sci 2005;45:1254–64.
[94] Jafari SH, Yavari A, Asadinezhad A, Khonakdar HA, Bohme F. Correlation of morphology and rheological response of interfacially modified PTT/m-LLDPE blends

with varying extent of modification. Polymer 2005;46: 5082–93.
[95] Bourry D, Favis BD. Cocontinuity and phase inversion in HDPE/PS blends: influence of interfacial modification and elasticity. J Polym Sci B 1998;36:1889–99.
[96] Cheng S-K, Wang C-C, Chen C-Y. Study on the phase behavior of EVA/PS blends during in situ polymerization. Polym Eng Sci 2003;43:1221–31.
[97] Veenstra HJJ, van Lent B, van Dam J, Posthuma de Boer A. Co-continuous morphologies in polymer blends with SEBS block copolymers. Polymer 1999;40:6661–72.
[98] Deimede VA, Fragou KV, Koulouri EG, Kallitsis JK, Voyiatzis GA. Miscibility behavior of polyamide 11/ sulfonated polysulfone blends using thermal and spectroscopic techniques. Polymer 2000;41:9095–101.
[99] Zheng S, Huang J, Liu W, Yang X, Guo Q. Miscibility and phase behaviour in blends of poly(vinyl alcohol) and a copolyamide. Eur Polym J 1996;32:757–76.
[100] Balsamo V, Calzadilla N, Mora G, Muller AJ. Thermal characterization of polycarbonate/polycaprolactone blends. J Polym Sci B 2001;39:771–85.
[101] Martuscelli E, Pracella M, Yue WP. Influence of composition and molecular mass on the morphology, crystallization and melting behavior of poly(ethylene oxide)/poly(methyl methacrylate) blends. Polymer 1984;25:1097–106.
[102] Shi Y, Jabarin SA. Glass-transition and melting behavior of poly(ethylene terephtalate)/poly(ethylene 2,6-naphthalate) blends. J Appl Polym Sci 2001;81:11–22.
[103] Nishi T, Wang TT. Melting point depression and kinetic effects of cooling on crystallization in poly(vinylidene fluoride)-poly(methyl methacrylate) mixtures. Macromolecules 1975;8:909–15.
[104] Gedde UW. Polymer physics. Boston: Kluwer; 1999. p. 169–98.
[105] Brandrup J, Immergut EH, editors. Polymer handbook. 3rd ed. New York: Wiley; 1989.
[106] Hoffman JD, Weeks JJ. Melting process and equilibrium melting temperature of poly(chlorotrifluoroethylene). J Res Nat Bur Standards 1962;66A(1):13–28.
[107] Castro M, Carrot C, Prochazka F. Experimental and theoretical description of low frequency viscoelastic behavior in immiscible polymer blends. Polymer 2004;45: 4095–104.
[108] Risch BG, Wilkes GL, Warakomski JM. Crystallization kinetics and morphological features of star-branched nylon-6: effect of branch-point functionality. Polymer 1993;34:2330–43.
[109] Painter PC, Coleman MM. Fundamentals of polymer science. 2nd ed. Lancaster: Technomic; 1997.
[110] Eguiburu JL, Iruin JJ, Fernandez-Berridi MJ, San Roman J. Blends of amorphous and crystalline polylactides with poly(methyl methacrylate) and poly(methyl acrylate): a miscibility study. Polymer 1998;39:6891–6.
[111] Wadey BL. Plasticizers. In: Meyers R, editor. Encyclopedia of physical science and technology. New York: Academic Press; 2001.
[112] Nielsen LE, Landel RF. Mechanical properties of polymers and composites. 2nd ed. New York: Marcel Dekker; 1994.
[113] Baiardo M, Frisoni G, Scandola M, Rimelen M, Lips D, Ruffieux K, et al. Thermal and mechanical properties of plasticized poly(L-lactic acid). J Appl Polym Sci 2003;90: 1731–8.
[114] Jacobsen S, Fritz HG. Plasticizing polylactide—the effect of different plasticizers on the mechanical properties. Polym Eng Sci 1999;39:1303–10.
[115] Ash BJ, Siegel RW, Schadler LS. Mechanical behavior of alumina/poly(methyl methacrylate) nanocomposites. Macromolecules 2004;37:1358–69.
[116] Ash BJ, Siegel RW, Schadler LS. Glass-transition temperature behavior of alumina/PMMA nanocomposites. J Polym Sci B 2004;42:4371–83.
[117] Li GZ, Cho H, Wang L, Toghiani H, Pittman Jr. CU. Synthesis and properties of poly(isobutyl methacrylate-co-butanediol dimethacrylate-co-methacryl polyhedral oligomeric silsesquioxane) nanocomposites. J Polym Sci, Part A 2005;43:355–72.
[118] Alegria A, Colmenero J, Ngai KL, Roland CM. Observation of the component dynamics in a miscible polymer blend by dielectric and mechanical spectroscopies. Macromolecules 1994;27:4486–92.
[119] Alvarez F, Alegria A, Colmenero J. Study of the two-component segmental dynamics of poly(vinylethylene)/ polyisoprene miscible blends. Macromolecules 1997;30: 597–604.
[120] Dionisio MCS, Ramos JJM, Fernandes AC. Dielectric studies on the miscibility in poly(vinyl acetate)/poly(ethyl methacrylate) blends. J Appl Polym Sci 1996;60:903–9.
[121] Madbouly SA, Otaigbe JU, Hassan MK, Mauritz KA. Broadband dielectric spectroscopy of mPP/PC blend prepared via in situ polymerization and compatibilization. Am Chem Soc Polym Mater Sci Eng 2006;94:831–2.
[122] Pratt GJ, Smith MJA. A dielectric investigation of miscibility and morphology in engineering thermoplastics. Polym Int 1997;43:137–42.
[123] Perrin FX, Nguyen VN, Vernet JL. Dielectric study of the effect of a sol–gel inorganic network on polymeric relaxation dynamics in acrylic/titania hybrids. Macromol Chem Phys 2005;206:1439–47.
[124] Davis RD, Bur AJ, McBrearty M, Lee Y-H, Gilman JW, Start PR. Dielectric spectroscopy during extrusion processing of polymer nanocomposites: a high throughput processing/characterization method to measure layered silicate content and exfoliation. Polymer 2004;45:6487–93.
[125] Lee Y-H, Bur AJ, Roth SC, Start PR. Accelerated alpha relaxation dynamics in the exfoliated Nylon-11/clay nanocomposite observed in the melt and semicrystalline state by dielectric spectroscopy. Macromolecules 2005;38:3828–37.
[126] Frank B, Frubing P, Pissis P. Water sorption and thermally stimulated depolarization currents in Nylon-6. J Polym Sci B: Polym Phys 1996;34:1853–60.
[127] Laredo E, Grimau M, Sanchez F, Bello A. Water absorption effect on the dynamic properties of Nylon-6 by dielectric spectroscopy. Macromolecules 2003;36:9840–50.
[128] Laredo E, Hernandez MC. Moisture effect on the low- and high-temperature dielectric relaxations in Nylon-6. J Polym Sci B 1997;35:2879–88.
[129] McCrum NG, Read BE, Williams G. Anelastic and dielectric effects in polymeric solids. New York: Dover; 1991. p. 617.
[130] O'Reilly JM, Papadopoulos K. Novel organic–inorganic glasses. J Mater Sci 2001;36:1595–600.
[131] Liu Y, Donovan JA. Miscibility and crystallizationf of semicrystalline nylon 6 and amorphous nylon 6IcoT blends. Polymer 1995;36:4797–803.

[132] Zhang SH, Jin X, Painter PC, Runt J. Composition-dependent dynamics in miscible polymer blends: influence of intermolecular hydrogen bonding. Polymer 2004;45: 3933–42.
[133] Havriliak S, Negami S. A complex plane representation of dielectric and mechanical relaxation processes in some polymers. J Polym Sci Polym Symp 1966;14:161–210.
[134] Kryitsis A, Pissis P, Grigorieva OP, Sergeeva LM, Brouko AA, Zimich ON, et al. Structure-property relationships in thermoplastic-apparent interpenetrating polymer networks based on crystallizable polyurethane and styrene-acrylic acid copolymer. J Appl Polym Sci 1999;73:385–97.
[135] [a] Shafee EE. Investigation of the phase structure of poly(3-hydroxybutyrate)/poly(vinyl acetate) blends by dielectric relaxation spectroscopy. Eur Polym J 2001;37: 451–8;
[b] Urman K, Madbouly S, Otaigbe JU. Unusual accelerated molecular relaxations of a tin fluorophosphate glass/polyamide 6 hybrid studied by broadband dielectric spectroscopy. Polymer 2006;48:1659–66.
[136] Runt JP, Fitzgerald JJ, editors. Dielectric spectroscopy of polymeric materials: fundamentals and applications. American Chemical Society Symposium Series 461. Washington, DC: American Chemical Society; 1997.
[137] Schmidt-Rohr K, Rawal A, Fang X-W. A new NMR method for determining the particle thickness in nanocomposites using $T_{2,H}$-selective $X\{^1H\}$ recoupling. J Chem Phys 2007;126. 054701/1–054701/16.
[138] [a] Rawal A, Urman K, Otaigbe JU, Schmidt-Rohr K. Detection of nanometer-scale mixing in phosphate-glass/polyamide-6 hybrids by 1H-31P NMR. Chem Mater 2006;18:6333–8;
[b] Zabel H. Quasi-elastic scattering: a powerful tool for investigating diffusion in solids. In: Murch GE, Birnbaum HK, Cost JR, editors. Nontraditional methods in diffusion. AIME publication; 1984.
[139] Kim J, Zhou H, Nguyen ST, Torkelson JM. Synthesis and application of styrene/4-hydroxystyrene gradient copolymers made by controlled radical polymerization: compatibilization of immiscible polymer blends via hydrogen-bonding effects. Polymer 2006;47:5799–809.
[140] Kolarik J, Fambri L, Slouf M, Konecny D. Heterogeneous polyamide 66/syndiotactic polystyrene blends: phase structure and thermal and mechanical properties. J Appl Polym Sci 2005;96:673–84.
[141] Lee SY, Kim SC. Effect of compatibilizer on the crystallization, rheological, and tensile properties of LDPE/EVOH blends. J Appl Polym Sci 1998;68:1245–56.
[142] Qui Z, Yang W. Crystallization kinetics and morphology of poly(butylene succinate)/poly(vinyl phenol) blend. Polymer 2006;47:6429–37.
[143] Sarasua JR, Arraiza AL, Balerdi P, Maiza I. Crystallinity and mechanical properties of optically pure polylactides and their blends. Polym Eng Sci 2005;45:743.
[144] Wilkinson AN, Tattum SB, Ryan AJ. Inhibition of crystalline structure development in a reactive polycarbonate-poly(butylene terephthalate) blend. Polym Bull 2002;48:199–206.
[145] Tol RT, Mathot VBF, Groeninckx G. Confined crystallization phenomena in immiscible polymer blends with dispersed micro- and nanometer sized PA6 droplets. Part 3: crystallization kinetics and crystallinity of micro- and nanometer sized PA6 droplets crystallizing at high supercoolings. Polymer 2005;46:2955–65.
[146] Chen C, Yu PHF, Cheung MK. Hydrogen bonding, miscibility, crystallization, and thermal stability in blends of biodegradable polyhydroxyalkanoates and polar small molecules of 4-tert-butylphenol. J Appl Polym Sci 2005; 98:736–45.
[147] Peng S, An Y, Chen C, Fei B, Zhuang Y, Dong L. Miscibility and crystallization behavior of poly(3-hydroxybutyrate-co-3-hydroxyvalerate)/poly(propylene carbonate) blends. J Appl Polym Sci 2003;90:4054–60.
[148] Akiba I, Akiyama S. Phase diagram of Poly(4-vinylphenol)-*N*,*N* dimethyloctadecylamine mixture. Macromolecules 1999;32:3741–5.
[149] Habenschuss A, Varma-Nair M, Kwon YK, Ma J, Wunderlich B. The phase diagram of poly(4-hydroxybenzoic acid) and poly(2,6-hydroxynaphthoic acid) and their copolymers from X-ray diffraction and thermal analysis. Polymer 2006;47:2369–80.
[150] Park J-Y, Kim D, Harris FW, Cheng SZD. Phase structure, morphology and phase boundary diagram in an aromatic polyimide (BPDA-PFMB)/m-cresol system. Polym Int 1995;37:207–14.
[151] Horst R, Wolf BA. Calculation of shear influences on the phase separation of polymer blends exhibiting upper critical solution temperatures. Rheol Acta 1994;33: 99–1071.
[152] Krause C, Horst R, Wolf BA. Shear effects on the phase diagrams of solutions of highly incompatible polymers in a common solvent. 2. Experiment and theory. Macromolecules 1997;30:885–9.
[153] Madbouly SA. Binary miscible blends of poly(methyl mehtacrylate)/poly(alpha-methyl styrene-co-acrylonitrile). IV. Relationship between shear flow and viscoelastic properties. J Macromol Sci—Phys 2003;42:1209–23.
[154] Madbouly SA, Chiba T, Ougizawa T, Inoue T. Shear effect on the phase behavior and morphology in PMMA/SAN-29.5 blend. J Macromol Sci—Phys 1999;38(1 and 2): 79–92.
[155] Madbouly SA, Ohmomo M, Ougizawa T, Inoue T. Effect of the shear flow on the phase behavior of polystyrene/poly(vinyl methyl ether) blend. Polymer 1999;40:1465–72.
[156] Madbouly SA, Wolf BA. Shear-induced crystallization and shear-induced dissolution of poly(ethylene oxide) in mixtures with tetrahydronaphthalene and oligio(dimethyl siloxane-b-ethylene oxide). Macromol Chem Phys 2003; 204:417–24.
[157] Agarwal PK, Somani RH, Weng W, Mehta A, Yang L, Ran S, et al. Shear-Induced cyrstallization in novel long chain branched polypropylenes by in situ Rheo-SAXS and -WAXD. Macromolecules 2003;36:5226–35.
[158] Yang L, Somani RH, Sics I, Hsiao BS, Kolb R, Fruitwala H, et al. Shear-induced crystallization precursor studies in model polyethylene blends by in situ Rheo-SAXS and Rheo-WAXD. Macromolecules 2004;37:4845–59.
[159] Malwitz MM, Butler PD, Porcar L, Angelette DP, Schmidt G. Orientation and relaxation of polymer-clay solutions studied by rheology and small-angle neutron scattering. J Polym Sci B 2004;42:3102–12.
[160] Mortensen K, Theunissen E, Kleppinger R, Almdal K. Shear-induced morphologies of cubic ordered block copolymer micellar networks studied by in situ small-angle

neutron scattering and rheology. Macromolecules 2002;35:7773–81.

[161] Crist B. Thermodynamic interactions in isotope blends: experiment and theory. Macromolecules 1998;31:5853–60.

[162] Lee JS, Foster MD, Wu DT. Effects of branch points and chain ends on the thermodynamic interaction parameter in binary blends of regularly branched and linear polymers. Macromolecules 2006;39:5113–21.